forests

MDPI

Article

UAV Flight Orientation and Height Influence on Tree Crown Segmentation in Agroforestry Systems

Juan Rodrigo Baselly-Villanueva [1,*], Andrés Fernández-Sandoval [1], Sergio Fernando Pinedo Freyre [1], Evelin Judith Salazar-Hinostroza [2], Gloria Patricia Cárdenas-Rengifo [3], Ronald Puerta [4], José Ricardo Huanca Diaz [5], Gino Anthony Tuesta Cometivos [5], Geomar Vallejos-Torres [6], Gianmarco Goycochea Casas [7], Pedro Álvarez-Álvarez [8,*] and Zool Hilmi Ismail [9]

1 Estación Experimental Agraria San Roque, Instituto Nacional de Innovación Agraria (INIA), Calle San Roque 209, Loreto 16430, Peru; afernandez@inia.gob.pe (A.F.-S.); spinedo@inia.gob.pe (S.F.P.F.)
2 Dirección de Desarrollo Tecnológico Agrario, Instituto Nacional de Innovación Agraria (INIA), Av. La Molina 1981, Lima 15024, Peru; esalazar@inia.gob.pe
3 Estación Experimental Agraria Pucallpa, Instituto Nacional de Innovación Agraria (INIA), Carretera Federico Basadre Km 4200, Pucallpa 25004, Peru; gcardenas@inia.gob.pe
4 Universidad Nacional Agraria de la Selva, Tingo Maria, Huánuco 100601, Peru; ronald.puerta@unas.edu.pe
5 Universidad Nacional de la Amazonía Peruana (UNAP), Calle Pevas N° 548, Iquitos 16002, Peru; huancadiazjosericardo@gmail.com (J.R.H.D.); ginoanthony29@gmail.com (G.A.T.C.)
6 Universidad Nacional de San Martín, Jr. Maynas No 177, Tarapoto 22200, Peru; gvallejos@unsm.edu.pe
7 Department of Forest Engineering, Federal University of Viçosa, Viçosa 36570-900, MG, Brazil; gianmarco.casas@ufv.br
8 Department of Organisms and Systems Biology, Polytechnic School of Mieres, University of Oviedo, E-33600 Mieres, Asturias, Spain
9 Center for Artificial Intelligence and Robotics, Universiti Teknologi Malaysia, Jalan Sultan Yahya Petra, Kuala Lumpur 54100, Malaysia; zool@utm.my
* Correspondence: jrbasellyv@gmail.com (J.R.B.-V.); alvarezpedro@uniovi.es (P.Á.-Á.)

Abstract

Precise crown segmentation is essential for assessing structure, competition, and productivity in agroforestry systems, but delineation is challenging due to canopy heterogeneity and variability in aerial imagery. This study analyzes how flight height and orientation affect segmentation accuracy in an agroforestry system of the Peruvian Amazon, using RGB images acquired with a DJI Mavic Mini 3 Pro UAV and the instance-segmentation models YOLOv8 and YOLOv11. Four flight heights (40, 50, 60, and 70 m) and two orientations (parallel and transversal) were analyzed in an agroforestry system composed of *Cedrelinga cateniformis* (Ducke) Ducke, *Calycophyllum spruceanum* (Benth.) Hook.f. ex K.Schum., and *Virola pavonis* (A.DC.) A.C. Sm. Results showed that a flight height of 60 m provided the highest delineation accuracy (F1 ≈ 0.88 for YOLOv8 and 0.84 for YOLOv11), indicating an optimal balance between resolution and canopy coverage. Although YOLOv8 achieved the highest precision under optimal conditions, it exhibited greater variability with changes in flight geometry. In contrast, YOLOv11 showed a more stable and robust performance, with generalization gaps below 0.02, reflecting a stronger adaptability to different acquisition conditions. At the species level, vertical position and crown morphological differences (Such as symmetry, branching angle, and bifurcation level) directly influenced detection accuracy. *Cedrelinga cateniformis* displayed dominant and asymmetric crowns; *Calycophyllum spruceanum* had narrow, co-dominant crowns; and *Virola pavonis* exhibited symmetrical and intermediate crowns. These traits were associated with the detection and confusion patterns observed across the models, highlighting the importance of crown architecture in automated segmentation and the potential of UAVs

Academic Editors: Zixuan Qiu, Zhongke Feng and Huiqing Pei

Received: 10 November 2025
Revised: 4 January 2026
Accepted: 7 January 2026
Published: 9 January 2026

combined with YOLO algorithms for the efficient monitoring of tropical agroforestry systems.

Keywords: *Calycophyllum spruceanum*; *Cedrelinga cateniformis*; *Virola pavonis*; crown; forest monitoring; remote sensing; YOLO

1. Introduction

Tree crown architecture influences light interception, canopy structure, and competition, making crown characterization a key element for forest and agroforestry management [1]. In agroforestry systems, crown size and spatial arrangement regulate shading patterns that affect crop photosynthesis and biomass accumulation, thereby conditioning system productivity [2–5]. Consequently, accurate crown delineation is essential for both ecological assessment and management-oriented applications.

Traditionally, tree crown area has been estimated using ground-based measurements combined with geometric assumptions or optical methods such as hemispherical photography [6–8]. Although these approaches provide valuable information, they are time-consuming, require intensive field effort, and are susceptible to observer-related variability, limiting their applicability over large or structurally complex areas.

Recent advances in UAV (Unmanned Aerial Vehicle)-based remote sensing, particularly when integrated with AI-driven segmentation models, have substantially improved the accuracy and efficiency of crown measurements [9–11]. UAV platforms enable the acquisition of very high-resolution imagery at relatively low cost and with high operational flexibility, allowing for both fine-scale analysis of individual tree crowns and broader assessments of stand structure across forests and agroforestry landscapes [12,13]. As a result, UAV-based crown segmentation has become an indispensable tool for forest monitoring, driving the development of automated and scalable delineation methods [14,15].

Despite these advantages, individual tree crown (ITC) delineation in agroforestry systems remains highly challenging due to structural heterogeneity and mixed-species composition. Shaded coffee and cocoa plantations, silvopastoral systems, and mixed orchards often present overlapping canopies, variable crown density, complex shadow patterns, and fluctuating illumination, which obscure crown boundaries and reduce segmentation accuracy [16,17]. These difficulties are further intensified by interspecific differences in crown architecture, leaf phenology, and spectral response.

Several studies have shown that UAV flight height is a critical factor controlling the quality of individual tree crown detection and segmentation, mainly through its influence on ground sampling distance (GSD) and the apparent crown size in imagery [11,13,18]. Lower flight altitudes produce finer spatial resolution; however, excessively high image resolution does not necessarily improve deep learning performance, particularly in structurally heterogeneous canopies [13,18]. Conversely, higher flight altitudes (i.e., coarser spatial resolution) reduce the level of spatial detail available and may decrease detection and delineation accuracy [11,13]. Overall, these findings indicate a trade-off between spatial resolution and model performance, highlighting the need to identify a balanced or optimal flight height [11,18]. In addition, flight-line orientation relative to tree arrangement or crop row direction influences the quality of UAV-derived products; aligning flight paths with row direction can improve geometric and radiometric consistency and facilitate canopy structure characterization [19].

YOLO (You Only Look Once) is a one-stage object detection model that rapidly predicts bounding boxes and object masks in a single pass [20]. Beginning with YOLOv8, the architecture introduced an anchor-free detection head combined with advanced backbone

and neck designs, enhancing feature extraction and optimizing the balance between accuracy and speed [21].

Several studies have shown that YOLO model variants, both in their native implementations and in modified versions, offer competitive and often superior performance compared to widely used object detectors, particularly in terms of the trade-off between accuracy and inference speed. For instance, DS-YOLOv8 has demonstrated significant improvements in detecting small, multiple, and partially occluded targets through the incorporation of modules such as DCN_C2f (Deformable Convolutional Network with Cross-Stage Partial connections), SC_SA (spatial–channel self-attention), and the Wise-IoU loss function. These enhancements enabled DS-YOLOv8 to outperform models such as SSD (Single Shot MultiBox Detector), Faster R-CNN (Region-based Convolutional Neural Network), and earlier YOLO versions (v3 and v5) across several remote sensing benchmark datasets, including RSOD, NWPU VHR-10, DIOR, and VEDAI, while maintaining high processing speeds of approximately 93 fps [22]. Similarly, in weed detection applications, YOLOv9 achieved the highest mAP@0.5 values, whereas YOLOv11 provided the fastest inference times, surpassing two-stage detectors such as Faster R-CNN and demonstrating improved generalization under limited training data conditions [23]. In infrastructure inspection tasks, particularly for solar panel monitoring, YOLO-based architectures—especially YOLOv8-m—have also shown superior performance relative to traditional convolutional neural networks, achieving high levels of accuracy and sensitivity [24]. Collectively, these studies highlight the suitability of YOLO models for applications that require an efficient balance between accuracy, computational efficiency, and robustness in complex visual environments.

In general, the YOLO model has recently been increasingly applied to solve problems in forest sciences. For example, it has been used for the fast and accurate detection of dead trees in protected forests [25], as a real-time detector of structural defects in trees (such as cracks and holes) [26], and for the rapid and precise detection of forest fires [27]. It has also been applied for the individual detection of trees in forest environments using LiDAR data acquired from drones [28], for detecting and counting oil palm trees in high-resolution aerial images [29], and for identifying and quantifying shoots of *Eucalyptus* clones in plantation forests [30]. Furthermore, YOLO has been employed for the automatic detection of stacked *Eucalyptus* logs in storage yards using field video recordings [31,32].

Recent studies have applied YOLO models to tree detection in different Peruvian contexts. For instance, in the Peruvian Amazon, the use of UAV imagery combined with YOLO models has proven effective for detecting and delineating individual tree crowns in complex forest environments. One study focused on wax palms, a culturally and ecologically significant species, showing that YOLO architectures can adapt well to heterogeneous canopy structures and provide reliable results for species mapping and forest monitoring [33]. In urban contexts, deep learning models such as YOLOv5 have been successfully applied to aerial and ground-level images to detect and geolocate street trees [34]. Despite the high segmentation capacity, studies in agroforestry systems of the Peruvian Amazon remain scarce.

Agroforestry is especially prominent in the Peruvian Amazon, where it is promoted as a strategy to curb deforestation and improve sustainability on small farms [35]. The Amazon region's hot, humid climate (lowland rainforests and submontane forests) provides ideal conditions for diverse agroforestry systems. Smallholder farmers commonly establish multi-strata agroforests that mimic the structure of natural forests: perennial crops like cacao or coffee form an understory beneath a canopy of mixed tree species [36,37]. For example, cacao (*Theobroma cacao*) is typically grown under 50%–60% shade cover, which farmers achieve by planting fast-growing shade trees around the cacao rows

[38,39]. Coffee (*Coffea arabica*) is grown under a diversified shade canopy as part of agroforestry systems [40,41].

In the agroforestry systems of the Peruvian Amazon, a wide diversity of native tree species is commonly employed. *Calycophyllum spruceanum* (Benth.) Hook.f. ex K.Schum. (capirona) is valued in agroforestry systems (AFSs) for its rapid growth, high-quality timber, and its tall, well-defined crown, which allows for adequate light penetration for understory crops such as cacao and coffee. Its crown architecture, together with its condition as a light-demanding pioneer species, supports its use in restoration and silvicultural practices [42,43]. *Cedrelinga cateniformis* (Ducke) Ducke ("tornillo") plays a key role as an upper-canopy species in AFSs. Its broad and moderately dense crown provides intermediate shade that facilitates the coexistence of crops and pastures. Additionally, its rapid juvenile growth, high timber value, and contributions to microclimate regulation and system structure justify its frequent integration into agroforestry and silvopastoral arrangements [17,44–46]. *Virola pavonis* (A.DC.) A.C. Sm. ("cumala") is incorporated into AFSs, particularly in humid or flood-prone areas, due to its adaptation to waterlogged soils and its symmetrical crown architecture, which provides canopy stability and coverage. Its increasingly demanded timber adds economic value to its ecological function within the system [47].

Under this context, we hypothesize that both flight height and flight orientation significantly influence the accuracy of individual tree crown (ITC) segmentation in structurally heterogeneous agroforestry systems of the Peruvian Amazon. Previous studies have shown that image resolution and flight height strongly affect ITC detection and delineation in forests and plantations [13], but the combined effects of flight geometry and modern one-stage instance-segmentation models have not yet been systematically evaluated in tropical agroforestry canopies. Specifically, the objectives of this study were: (i) to quantify how UAV flight height and orientation jointly affect ITC segmentation accuracy in a multi-strata agroforestry system, (ii) to compare the performance and calibration behavior of YOLOv8 and YOLOv11 instance-segmentation models under these varying acquisition conditions, and (iii) to characterize the crown morphology of the forest species and analyze how these traits influence crown segmentation.

2. Materials and Methods

2.1. Study Site and Species

The study was carried out in an agroforestry system located in the Peruvian Amazon, specifically in the district of San Juan Bautista, province of Maynas, Loreto region. The reference coordinates are 3.939641° S and 73.418874° W, at an elevation of 116 m above sea level. The study area corresponds to the "El Dorado" Experimental Annex of the San Roque Agricultural Experimental Station, which is managed by the National Institute of Agricultural Innovation (INIA). In this area, a warm-humid climate typical of the lowland Amazon prevails, with temperatures ranging from 21 °C to 33 °C, an annual mean temperature of approximately 26–27 °C, and an annual precipitation of about 3000 mm, concentrated mainly between November and May [48]. The predominant soils exhibit clay-loam and loamy-sand textures, strong acidity (pH 4.5–4.77), and organic matter levels between 0.80% and 1.77%, categorized as low to moderate [44,49]. These edaphoclimatic attributes are characteristic of the lowland Amazonian terraces, geomorphological units formed by ancient alluvial deposits and defined by deep, highly weathered soils subjected to intense leaching due to the region's high rainfall. As a result, these soils exhibit low chemical fertility, accumulation of exchangeable aluminum, and moderate drainage, conditions that create humid and stable environments favorable for the development of barillal forests and agroforestry systems representative of the Peruvian Amazon.

The agroforestry system (AFS) was established on an area of 1 hectare and is 11 years old. The genetic material used for its establishment originated from botanical seeds collected from trees located in the natural forests surrounding the study area [50]. The system is composed of forest species such as *C. spruceanum* (49 individuals), *C. cateniformis* (92 individuals) and *V. pavonis* (81 individuals); along with a fruit species, *Theobroma cacao* L. (118 individuals) and a forage species, *Centrocema macrocarpum* Benth. The forest component was established following a rectangular planting design, with a spacing of 5 × 15 m between plants and rows; the fruit component was planted between the tree rows at 5 m intervals (Figure 1).

Structurally, the forest component exhibits a well-defined vertical stratification. *C. cateniformis* occupies the upper canopy layer and acts as the dominant species, presenting a diameter at breast height (DBH) of 26.07 ± 8.22 cm (8.6–43.2), a crown diameter (CD) of 7.74 ± 1.91 m (2.1–11.79), a crown height (CH) of 10.22 ± 2.11 m (5.7–15.8), and a total height (TH) of 16.16 ± 2.99 m (8.1–22). *C. spruceanum* forms the intermediate stratum, with a DBH of 15.93 ± 6.34 cm (4.6–30.2), a CD of 5.39 ± 2.55 m (1.1–11.81), a CH of 8.72 ± 2.81 m (2.8–16), and a TH of 13.14 ± 3.92 m (4.8–20.6). In contrast, *V. pavonis* occupies the lower stratum, with a DBH of 9.85 ± 5.67 cm (2.1–29.6), a CD of 3.18 ± 1.88 m (0.45–10.1), a CH of 4.06 ± 2.14 m (0.6–11), and a total height (TH) of 6.42 ± 3.08 m (0.9–15.4). These marked differences in size, crown architecture, and vertical position create a heterogeneous forest environment, providing a representative framework for evaluating and segmenting individual tree crowns under mixed canopies.

The methodological workflow for UAV-based individual tree crown segmentation in the agroforestry system is presented in Supplementary Figure S1. Experimental conditions were defined considering four flight heights (40–70 m) and two flight orientations (parallel and transversal), and RGB nadir images were acquired. The images were organized according to the flight configuration, and individual tree crowns were annotated using instance segmentation with the support of smart polygon tools and manual refinement; subsequently, the data were prepared through automatic orientation correction, resizing, and export to the YOLO format, and were split into training, validation, and test sets. YOLOv8 and YOLOv11 models were trained for each configuration and evaluated using precision, recall, F1-score, and AP@50 metrics, with optimal confidence thresholds selected. Finally, a comparative analysis was conducted by integrating field-assessed crown morphological traits through Multiple Correspondence Analysis (MCA) to evaluate the relationship between crown structure and segmentation performance.

2.2. UAV Image Acquisition

The aerial survey was conducted from 16 to 21 May 2025, under stable atmospheric conditions, with clear and sunny skies, between 11:00 a.m. and 1:00 p.m. The flights were carried out using a remotely piloted aircraft system (RPAS), model DJI Mavic Mini 3 Pro, equipped with an integrated RGB camera featuring a 1/1.3″ CMOS sensor, 12 MP resolution, f/1.7 aperture, and a fixed focal length of 8.8 mm [51]. The flights were configured with an 85% frontal (longitudinal) and lateral (transverse) overlap, ensuring the evaluation of all trees in the plot. The photographs were captured at the highest quality available on the equipment (4032 × 2268 pixels).

The planning and execution of the flights were carried out using the DroneLink application [52], installed on a mobile device connected to the aircraft's remote controller. The missions were flown at altitudes of 40, 50, 60, and 70 m, in two orientations relative to the row arrangement of the system: parallel (P), following the direction of the rows, and transversal (T), crossing the rows perpendicularly (Figure 1). Both orientations were included to account for potential differences associated with image acquisition geometry in row-based systems (i.e., the spatial arrangement of forest species within the agroforestry

system), which may influence crown visibility and segmentation performance under different illumination and viewing conditions. Rather than assuming visually evident differences in individual images, acquisitions in both flight directions were designed to systematically assess whether flight orientation affects model performance at different flight altitudes. Each height–orientation combination represented an independent dataset (e.g., "40-P", "50-T"), generating georeferenced RGB imagery suitable for individual tree analysis and stand-level mapping (Figure 1). Table 1 presents the operational characteristics of each combination of flight height and orientation. Mission durations ranged from 6 min and 58 s to 14 min and 53 s, depending on the programmed altitude and the number of flight paths required. These missions captured between 117 and 343 images, while the spatial resolution (GSD) ranged from 1.08 to 1.89 cm/pixel, demonstrating the direct relationship between flight height and the level of detail obtained in the imagery.

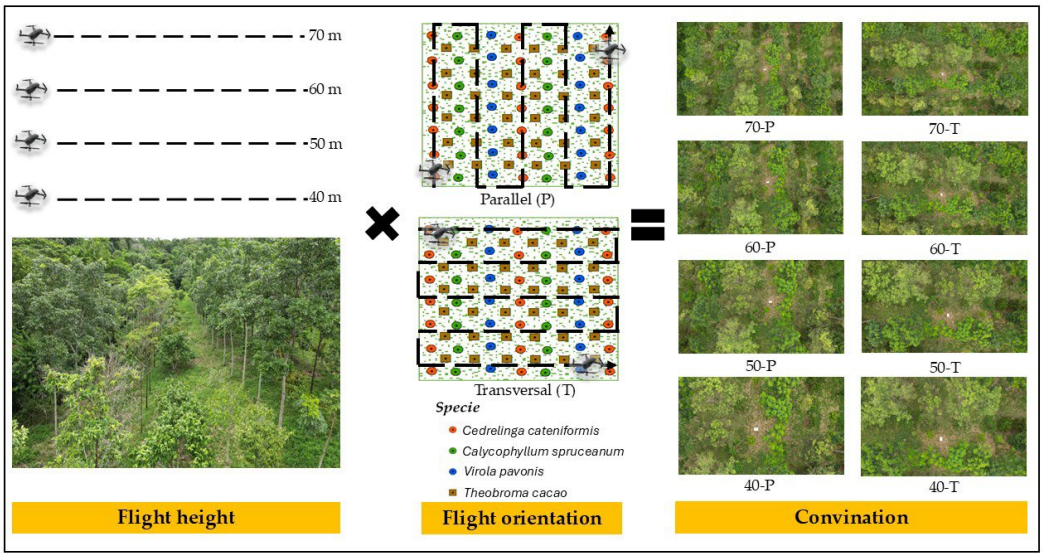

Figure 1. Flight design developed to evaluate the effect of flight height (40, 50, 60, and 70 m) and flight orientation relative to the row arrangement of the system (parallel—P and transversal—T) on crown segmentation quality. In the images, a rectangular white panel can be observed, which corresponds to a ground reference scale measuring 0.8 × 1.2 m and was used as a spatial reference in the study area.

Table 1. Operational characteristics of each combination of flight height and orientation for the detection of Amazonian tree crowns in agroforestry systems.

Flight Height (m)	Flight Orientation	Duration (mm:ss)	N° of Images	GSD (cm/Pixel)
70	Parallel	07:21	118	1.89
	Transversal	06:58	117	1.89
60	Parallel	08:54	165	1.62
	Transversal	08:03	159	1.62
50	Parallel	10:12	210	1.35
	Transversal	10:18	227	1.35
40	Parallel	14:53	343	1.08
	Transversal	14:06	331	1.08

2.3. Ground Truth and Dataset Organization

The photographs obtained during the flight missions were uploaded to the Roboflow server (https://app.roboflow.com), selecting the segmentation option for processing. Dataset was partitioned into 70% training, 20% validation, and 10% test, the split was performed at the image level (patch-based split), ensuring that each image was assigned exclusively to one of the three subsets. Individual tree crowns were annotated as instance-segmentation polygons using the Roboflow Annotate tool. The annotation process began with the Smart Polygon tool, which employs a Segment Anything–based model to generate an initial crown mask from a single click. Annotators evaluated the algorithmically generated contours in real time and refined them by adding or removing regions so that each mask accurately matched the crown boundaries visible in the UAV imagery. In cases where crowns exhibited irregular shapes, such as serrated margins, dispersed leaf clusters, or internal canopy gaps, the polygon complexity was increased to adequately capture these structural features. For larger crowns or in situations where Smart Polygon was unable to correctly delineate the boundaries, annotators provided a bounding box to guide the segmentation process.

When Smart Polygon could not effectively distinguish interlaced canopies or crowns with sparse foliage, the manual Polygon tool was used. At high magnification, annotators meticulously traced each crown vertex by vertex, following the contours of branches and foliage while ensuring clear separation between neighboring crowns to generate distinct, non-overlapping instances. This procedure prioritized accuracy over speed, as the precision of crown delineations would directly influence subsequent crown area estimations.

Annotations were performed independently for each flight height–orientation combination (e.g., 70-P, 70-T, 60-P, 60-T). Table 2 presents the number of annotated tree crown instances by flight height and orientation for *C. spruceanum*, *C. cateniformis*, and *V. pavonis*. Differences in the number of annotated crowns among the different configurations reflect variations in crown visibility and detection performance associated with image acquisition parameters, rather than differences in the surveyed area, as all datasets correspond to the same study site. The table shows that, at lower flight heights, the total number of annotated crowns tends to decrease, which is primarily related to the reduced spatial coverage per image. In contrast, higher flight heights provide greater spatial coverage, allowing a larger number of crowns to be included within each scene. In addition, the table highlights the effect of flight orientation on crown detectability at the same flight height, showing that parallel and transversal configurations do not provide the same level of visibility for all species, which underscores species-specific responses to image acquisition geometry.

Table 2. Number of annotated tree crowns by species, flight height, and flight orientation for the segmentation of Amazonian tree crowns in agroforestry systems.

Flight Height (m)	Flight Orientation	*C. spruceanum*	*C. cateniformis*	*V. pavonis*
70	Parallel	1483	2953	2177
	Transversal	1691	3171	2102
60	Parallel	2162	3720	3076
	Transversal	1191	2228	1572
50	Parallel	602	981	925
	Transversal	872	1524	1301
40	Parallel	248	433	402
	Transversal	404	680	612

2.4. Segmentation Models and Training

We trained instance-segmentation models for each flight condition (40, 50, 60 and 70 m; parallel and transversal) using two modern families that natively predict per-instance masks and class labels: YOLOv8 Segment (exposed in Roboflow 3.0 as Roboflow 3.0 Instance Segmentation) and YOLOv11 Segment. Both support mask-based instance segmentation and are commonly distributed in multiple sizes; we selected the Extra Large size to maximize accuracy, as Roboflow's recent guidance notes that the Extra Large configuration is the most accurate among the available sizes for detection and segmentation [53]. Adhering to pretraining-specific resizing and normalization steps significantly improves downstream task accuracy in remote sensing applications [54]. In our case, UAV images were resized to 640 × 640 pixels, and the Auto-Orient option was applied to correct image orientation based on EXIF metadata. This preprocessing step standardizes the resolution and visual orientation only, without altering the geometric content or the UAV flight path. The original 4032 × 2268 frames were uniformly rescaled to 640 × 640 pixels (not tiled or cropped), so tree crowns are not truncated by the input size. This input size follows the standard configuration recommended for YOLO models, providing a good balance between spatial detail and computational cost.

To shorten convergence and provide strong, generic boundary priors, each run was initialized from a public MS-COCO instance-segmentation checkpoint. In our training logs the checkpoint is recorded as COCOx-seg, corresponding to the best COCO segment model available in the gallery of public checkpoints (Best-Common Objects). Using a COCO-pretrained segment backbone is a standard practice for YOLO-based models and aligns with Ultralytics' distribution of weights that are pretrained on the COCO dataset [55].

2.5. Evaluation Metrics

The performance of the models was evaluated using standard instance-segmentation metrics, following the automated workflow provided by the Roboflow platform. During training, Roboflow automatically performed internal evaluation of each model after every epoch using the validation set, generating real-time precision (Equation (1)), recall (Equation (2)), and F1-score (Equation (3)) curves across the full range of confidence thresholds. The platform recommended an optimal confidence threshold that balances precision and recall; we adopted this operating point for each model–dataset pair. Final headline metrics were computed on the independent test set using the optimal-confidence threshold selected from validation. This workflow followed Roboflow's evaluation guidance on selecting the threshold that yields the best precision/recall/F1 trade-off for production. Furthermore, we also assessed Average Precision at 50% Intersection over Union (AP@50) (Equation (4)).

The training and validation learning curves (loss functions, precision, recall, and mAP) were analyzed to monitor the model's learning dynamics. This analysis provided insights into convergence behavior and performance stability, complementing the static evaluation metrics and ensuring a comprehensive assessment of detection and segmentation performance throughout the training process.

The corresponding mathematical formulations of the evaluation metrics are presented below:

Precision:

$$Precision = \frac{TP}{TP + FP} \quad (1)$$

Recall:

$$Recall = \frac{TP}{TP + FN} \quad (2)$$

where:

- True Positive (TP): a crown correctly predicted with sufficient overlap with the ground-truth mask.
- True Negative (TN): absence of a crown correctly predicted (less relevant in instance segmentation).
- False Positive (FP): a predicted crown with no corresponding ground-truth instance.
- False Negative (FN): a ground-truth crown missed by the model.

F1 Score:

$$F1 = \frac{2 \times Precision \times Recall}{Precision + Recall} \quad (3)$$

Average Precision at 50% Intersection over Union (AP@50)

$$AP@50 = \int_0^1 p(r)\ dr \quad \text{with} \quad IoU \geq 0.5 \quad (4)$$

where $p(r)$ is precision as a function of recall.

To evaluate model robustness, the generalization gap (G) was calculated as the absolute difference between the F1-scores obtained on the validation and test sets for each configuration (height × orientation × model), as defined in Equation (5). Small gap values indicate consistent performance across datasets and better generalization capability, whereas larger values reflect sensitivity to flight parameters and potential model instability.

$$G = |F1_{Validation} - F1_{Test}| \quad (5)$$

2.6. Comparative Analysis

To evaluate the effect of flight height and orientation on segmentation performance, we conducted a comparative analysis using the trained YOLOv8 and YOLOv11 models. First, we compared model performance across the four flight heights (40, 50, 60, and 70 m) and both flight orientations. For each height–orientation combination, we computed the average F1-score, precision, and recall to assess whether orientation affected crown delineation quality.

In addition, we calculated a generalization gap, defined as the absolute difference between validation and test F1-scores within the same agroforestry dataset, as an internal measure of model robustness under varying flight conditions. We then examined the relationship between F1-score and the optimal confidence threshold using scatterplots to characterize model calibration patterns and identify threshold ranges associated with balanced performance. The distributions of optimal confidence thresholds were also summarized with boxplots for validation and test sets to compare calibration consistency across models, heights, and orientations.

Finally, we evaluated species-level performance for *C. cateniformis*, *C. spruceanum*, and *V. pavonis*. Because these species differ in crown architecture and canopy density, reporting species-specific metrics allowed us to determine how crown structure influenced segmentation accuracy. For the best-performing flight height, confusion matrices were generated to analyze classification accuracy at the species level. All line plots, heatmaps, scatterplots, and boxplots were produced in RStudio (v. 4.3.3) [56] using the ggplot2 package [57].

2.7. Crown Morphological Assessment and Integration with UAV Segmentation Accuracy

The morphological characterization of the crowns of the three species studied was performed using Multiple Correspondence Analysis (MCA). This multivariate technique is suitable for simultaneously examining categorical variables and exploring structural patterns in qualitative data sets, making it a more appropriate alternative than methods such as PCA, which require continuous data and linear relationships.

The morphological dataset consisted of 259 individuals belonging to *C. spruceanum*, *C. cateniformis* and *V. pavonis*, evaluated in the field using a standardized protocol. For each tree, five categorical variables related to crown architecture were recorded, based on descriptors adapted from Galera et al. [58] and Kong et al. [59] variables were evaluated:

1. **Vertical structure:** Suppressed, intermediate, codominant, and dominant.
2. **Bifurcation position**, recorded according to its height relative to the crown: lower third, middle third, upper third or absence of bifurcation.
3. **Crown symmetry**, Classified as asymmetric (uneven distribution of branches around the trunk) or symmetric (equal lateral extension).
4. **Branching angle**, Right (branch insertion close to 90°), intermediate (branch insertion between 30° and 60°), or acute (branch insertion less than 30°).
5. **Branch thickness**, expressed as the relative diameter of branches to trunk insertion: thick (>50%), medium (25%–50%), or thin (<25%).

All variables were recoded as factors prior to the analysis to ensure their correct interpretation within the MCA framework. The analysis was performed using the MCA function from the FactoMineR package in RStudio [56]. This procedure generated a factorial space in which individuals (trees) were represented as points and the categories of each variable as vectors, allowing for the visualization of the joint structure of the dataset and the identification of morphological groupings among species. The results were visualized through a biplot generated with the fviz_mca_biplot function from the factoextra package [60], where a color scheme was applied for each species and clustering ellipses were added to facilitate the interpretation of structural affinities.

Finally, the patterns identified through the MCA were examined alongside the performance metrics obtained from the YOLOv8 and YOYOv11 models. This comparison allowed us to identify elements of crown architecture associated with segmentation accuracy and cross-species confusion trends. In this way, the MCA provided a complementary framework to understand how morphology influences detectability in UAV imagery and the behavior of crown segmentation models.

3. Results

3.1. Effect of Flight Height and Orientation on Model Performance

The evaluation of segmentation performance across different flight heights and orientations revealed clear patterns in both models (Table 3 and Figure 2). At 40 m height, performance differences between models and orientations were evident. YOLOv11 in parallel orientation achieved relatively high and balanced accuracy, with F1-scores of 0.812 in validation and 0.805 in testing, supported by precision and recall values around 0.80. In contrast, its transversal configuration produced notably lower results (0.743 and 0.744). YOLOv8 showed the opposite pattern: parallel orientation yielded its lowest performance (0.739 and 0.737), while transversal orientation improved results to 0.767 in validation and 0.797 in testing, indicating that orientation played a decisive role at this height.

At 50 m, YOLOv11 demonstrated stable behavior across orientations, with parallel runs reaching 0.815 and 0.820 in F1-scores, and transversal runs slightly higher (0.817 and 0.824). YOLOv8, however, displayed greater variability: while transversal orientation produced competitive results (0.799 and 0.814), parallel orientation dropped considerably,

with F1-scores of 0.770 in validation and only 0.712 in testing, highlighting the model's sensitivity to flight geometry at this height.

At 60 m, both models achieved their highest accuracy. YOLOv8 in parallel orientation reported the overall maximum across the study (F1 = 0.878 in validation; 0.886 in testing), with precision and recall values of 0.896 and 0.878, respectively. Its transversal configuration also performed strongly (0.849 and 0.852). Similarly, YOLOv11 showed substantial improvements at this height, reaching 0.837 and 0.832 in parallel, and slightly higher values in transversal (0.856 and 0.843). These results confirm 60 m as the optimal height, offering the best balance between crown detail and canopy coverage.

At 70 m, performance remained robust but slightly lower than at 60 m. YOLOv11 maintained comparable results in both orientations, with F1-scores around 0.813, while YOLOv8 achieved similar outcomes in parallel (0.797 and 0.813) and slightly superior results in transversal (0.818 and 0.832).

Table 3. Performance metrics of Yolov8 and Yolov11 as a function of flight height and orientation in the detection of amazonian tree crowns.

Height	Orientation	Model	Validation			Test		
			F1 Score	Precision	Recall	F1 Score	Precision	Recall
40	Parallel	YOLOv11	0.8120	0.8310	0.7920	0.8050	0.8020	0.8130
		YOLOv8	0.7390	0.7780	0.8010	0.7370	0.7920	0.6920
	Transversal	YOLOv11	0.7430	0.8520	0.7980	0.7440	0.7680	0.7280
		YOLOv8	0.7670	0.8670	0.7170	0.7970	0.8130	0.7820
50	Parallel	YOLOv11	0.8150	0.8480	0.8010	0.8200	0.8630	0.7830
		YOLOv8	0.7700	0.8300	0.8370	0.7120	0.6980	0.7270
	Transversal	YOLOv11	0.8170	0.8480	0.8190	0.8240	0.8910	0.7700
		YOLOv8	0.7990	0.8450	0.7830	0.8140	0.8690	0.7670
60	Parallel	YOLOv11	0.8370	0.8990	0.9280	0.8320	0.8100	0.8560
		YOLOv8	0.8780	0.8910	0.9110	0.8860	0.8960	0.8780
	Transversal	YOLOv11	0.8560	0.8980	0.8610	0.8430	0.8700	0.8210
		YOLOv8	0.8490	0.8740	0.8650	0.8520	0.9060	0.8070
70	Parallel	YOLOv11	0.7930	0.8400	0.8950	0.8130	0.8100	0.8170
		YOLOv8	0.7970	0.8640	0.8840	0.8130	0.8380	0.7900
	Transversal	YOLOv11	0.7980	0.8560	0.8190	0.8130	0.8300	0.7980
		YOLOv8	0.8180	0.8670	0.7940	0.8320	0.8780	0.7930

Taken together, the results highlight two complementary patterns: YOLOv8 reached the highest absolute accuracy under optimal conditions (60 m, parallel) but exhibited greater fluctuations across height, particularly at 40 and 50 m. YOLOv11, by contrast, did not achieve the same peak values but offered more stable and consistent performance, with F1-scores above 0.80 in nearly all scenarios. The heatmap (Figure 3) shows the absolute difference between validation and test F1-scores (generalization gap) for YOLOv8 and YOLOv11 across flight heights and orientations. Lower values indicate better generalization (i.e., more consistent performance between validation and test).

Results reveal a marked contrast between models. YOLOv11 consistently exhibited very small gaps (0.001–0.020) across all scenarios, confirming its robustness and stable calibration. Even at challenging heights (e.g., 40 m transversal or 70 m parallel), differences between validation and test remained minimal (<0.02), highlighting the model's ability to maintain reliable accuracy across acquisition conditions. By contrast, YOLOv8 displayed higher variability, with gaps ranging from as low as 0.003 (60 m transversal) to as high as 0.058 (50 m parallel). These fluctuations confirm its sensitivity to flight

parameters: while YOLOv8 reached the overall maximum accuracy (F1 = 0.886 at 60 m parallel), it also suffered larger discrepancies between validation and test at lower or intermediate heights.

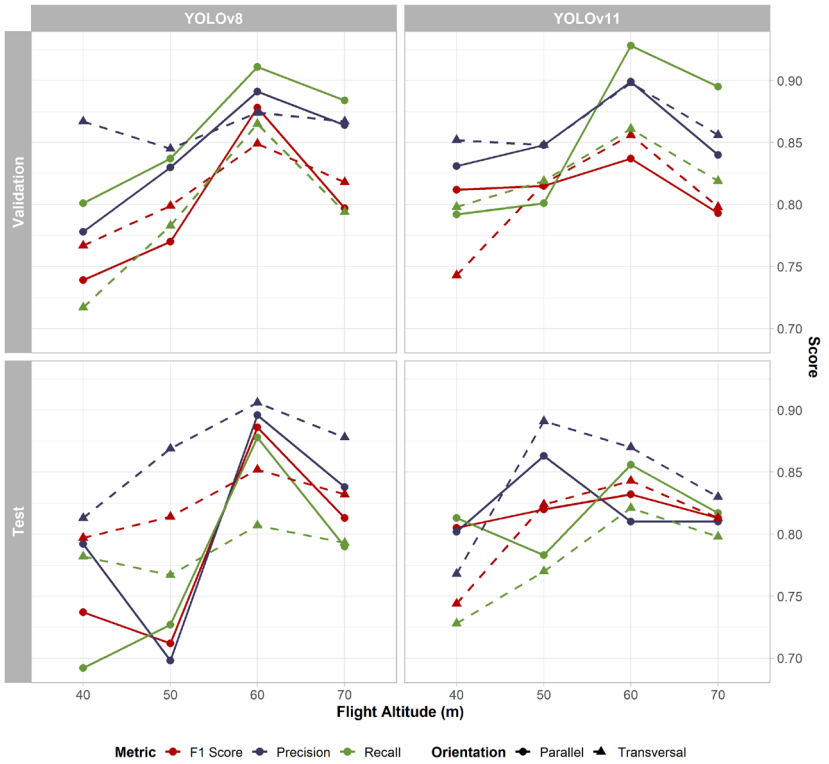

Figure 2. Comparative performance of YOLOv8 and YOLOv11 instance segmentation models across flight heights (40, 50, 60, and 70 m) and orientations (parallel vs. transversal) in agroforestry crown delineation tasks. Each panel shows validation or test results, with F1 score, precision, and recall reported as functions of height and flight orientation.

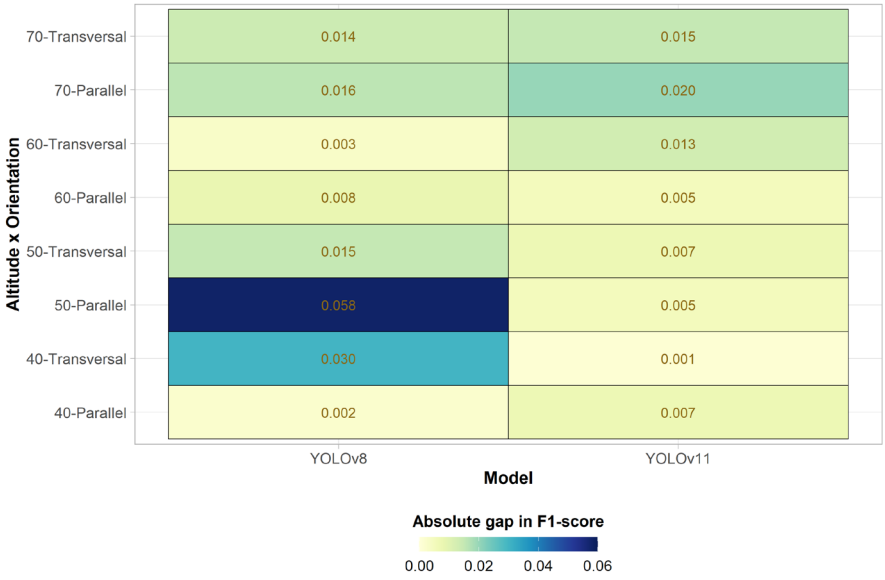

Figure 3. Heatmap of the generalization gap (absolute difference between validation and test F1-scores) for YOLOv8 and YOLOv11 across flight heights (40–70 m) and orientations (parallel vs. transversal).

Supplementary Figure S2 summarizes the training dynamics at 60 m flight altitude. YOLOv8 exhibited smooth and stable convergence in both orientations, with steadily decreasing training and validation losses and precision and recall consistently above 0.85, indicating robust learning stability and minimal overfitting. YOLOv11 showed less stable convergence patterns overall, particularly under transversal orientation, where fluctuations in validation losses and metrics were more evident. Nevertheless, its parallel orientation achieved smooth and consistent convergence, approaching the stability observed in YOLOv8 and yielding competitive final precision, recall, and mAP values.

3.2. Effect of Confidence Threshold on Model Performance

These results show that confidence threshold calibration differed fundamentally between models. The scatterplots with trend lines (Figure 4) show distinct relationships between the F1-score and the optimal confidence threshold for the two models. YOLOv8 exhibited a strong inverse association: its highest F1-scores were achieved when thresholds were set at very low values (often below 10%), while configurations requiring higher thresholds (>60%) corresponded to lower F1 performance. This pattern suggests that YOLOv8 maximized recall by allowing predictions with relatively low confidence to be retained but at the cost of unstable calibration across conditions. In contrast, YOLOv11 displayed a more balanced and consistent behavior. In the validation set, confidence thresholds remained largely independent of F1 performance, while in the test set the relationship was only mildly negative. This indicates that YOLOv11 maintained reliable performance without requiring extreme adjustments to the threshold.

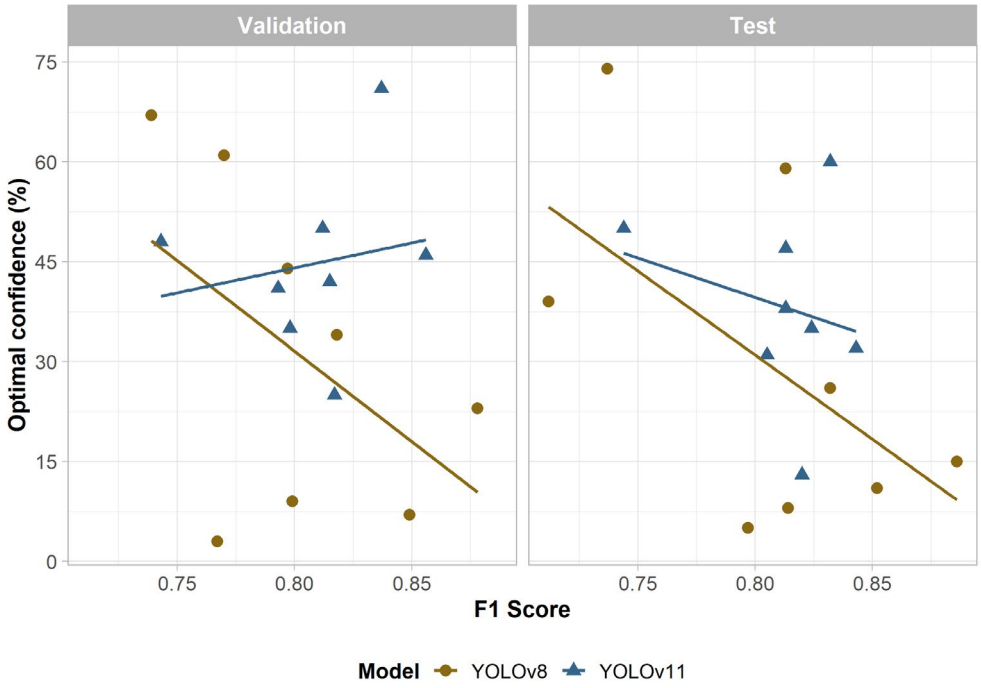

Figure 4. Scatterplots showing the relationship between F1-score and optimal confidence thresholds for YOLOv8 and YOLOv11 across validation (**left**) and test (**right**) sets. Regression lines highlight contrasting calibration patterns: YOLOv8 exhibits a strong negative association, requiring low thresholds to reach higher F1-scores, while YOLOv11 maintains more stable confidence ranges with weaker dependence on F1.

The boxplots (Figure 5) highlight these contrasting calibration dynamics. YOLOv11 demonstrated compact and well-defined distributions of optimal confidence values, with interquartile ranges consistently clustered around 35%–45% for both validation and test.

This narrow spread reflects stable calibration, meaning that YOLOv11 could operate effectively under a relatively fixed confidence regime regardless of flight height or orientation. By contrast, YOLOv8 displayed markedly broader distributions, with thresholds ranging from as low as 3%–5% in transversal orientations to over 70% in parallel flights at lower heights. Such wide variability underscores its sensitivity to acquisition parameters: although YOLOv8 achieved the single highest F1-score in the study (0.886 at 60 m parallel), this performance came at the expense of requiring highly variable thresholds that may limit operational robustness.

An F-test comparing the variances of F1-scores confirmed that YOLOv8 exhibited higher variability than YOLOv11 in both validation ($\sigma^2 = 0.0021$ vs. 0.0011) and test sets ($\sigma^2 = 0.0033$ vs. 0.0009), although the differences were not statistically significant ($p > 0.05$).

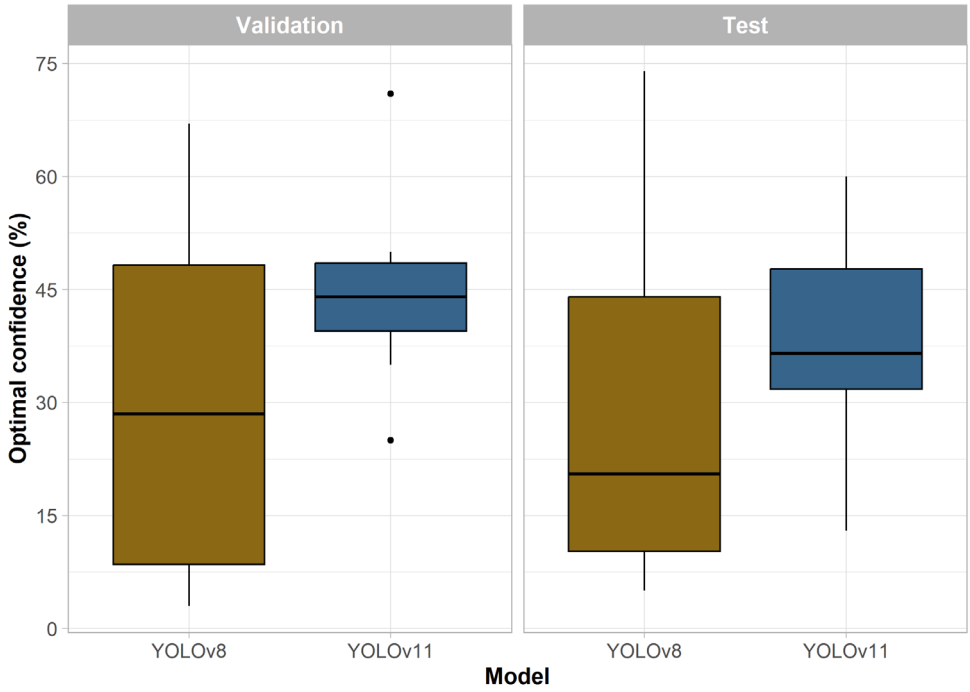

Figure 5. Boxplots of optimal confidence thresholds for YOLOv8 and YOLOv11 in validation (**left**) and test (**right**) sets. YOLOv11 displays compact and consistent distributions (interquartile range ~35%–45%), reflecting robust calibration, whereas YOLOv8 shows wider variability (3%–70%) depending on flight height and orientation, underscoring its sensitivity to acquisition conditions.

Supplementary Figure S3 shows how F1, precision, and recall vary with confidence threshold in validation (left) and test (right) sets. YOLOv8 reached its best F1-scores at very low thresholds (7%–23%), particularly in transversal flights, reflecting its recall-oriented calibration. In contrast, YOLOv11 achieved optimal balance at moderate thresholds (46%–71%), indicating more stable and consistent calibration across orientations.

3.3. Species-Specific Performance Across Heights and Orientations

Figure 6 summarizes the species-level AP@50 across flight heights and orientations for both YOLOv8 and YOLOv11, in validation (bottom panels) and test sets (top panels). Clear trends emerged, with the highest accuracies consistently observed at 60 m, regardless of model or species. For instance, in the test set, both YOLOv8 and YOLOv11 reported peak AP@50 values above 95% for *C. spruceanum* and *C. cateniformis* under parallel orientation, while *V. pavonis* also reached competitive results (>90%) at this height.

At lower heights (40–50 m), performance showed greater variability across species and orientations. In the validation set, YOLOv8 exhibited a marked decline in *C.*

spruceanum under transversal flights at 40 m (AP@50 < 80%), while YOLOv11 showed more balanced results, maintaining values closer to 85%–90% for most species. At 70 m, AP@50 values remained high for all species (>85%) in both validation and test, but a slight decrease relative to 60 m confirmed that the intermediate height provided the best balance between crown resolution and canopy coverage.

YOLOv11 consistently displayed smoother and more stable responses across heights, whereas YOLOv8 achieved the highest absolute peaks in the test set but also exhibited stronger fluctuations depending on species and orientation. These patterns highlight that, although species morphology (broad crowns vs. emergent forms) influenced detection accuracy, flight height was the dominant factor, with 60 m consistently outperforming other settings.

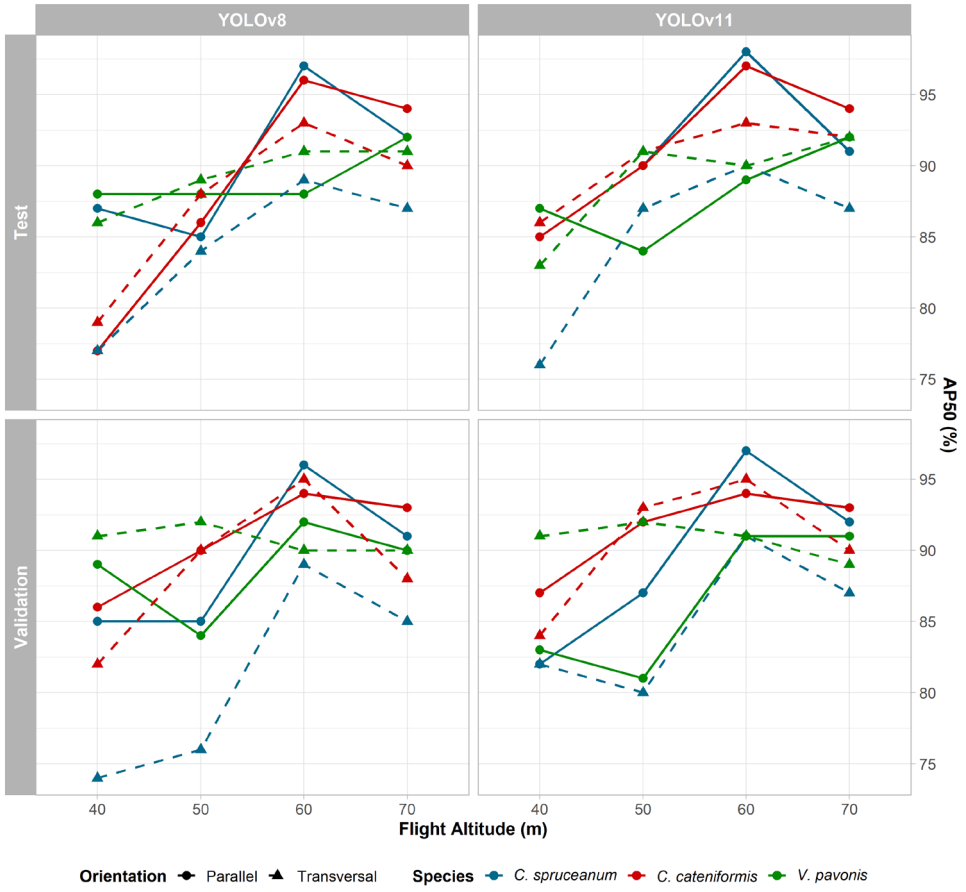

Figure 6. Species-specific crown segmentation accuracy (AP@50) of YOLOv8 and YOLOv11 models under agroforestry conditions, evaluated across flight heights (40, 50, 60, and 70 m) and orientations (parallel vs. transversal). Results are reported for both validation and test datasets, with separate panels for each model showing performance on *C. spruceanum*, *V. pavonis* and *C. cateniformis*.

Figure 7 compares the species-level confusion matrices for YOLOv8 and YOLOv11 at 60 m flight altitude, expressed as percentages. Both models correctly classified the majority of crowns for *C. cateniformis*, which consistently showed the highest diagonal values in both validation and test sets, reflecting its distinctive and well-defined crown morphology. For YOLOv8, detection of *C. spruceanum* and *V. pavonis* was also strong but exhibited slightly higher confusion, particularly under transversal orientation. In contrast, YOLOv11 produced more balanced results across species, with fewer drastic changes between validation and test sets. Its parallel orientation achieved the most consistent

performance, maintaining high true-positive rates for all three species and minimal cross-class confusion.

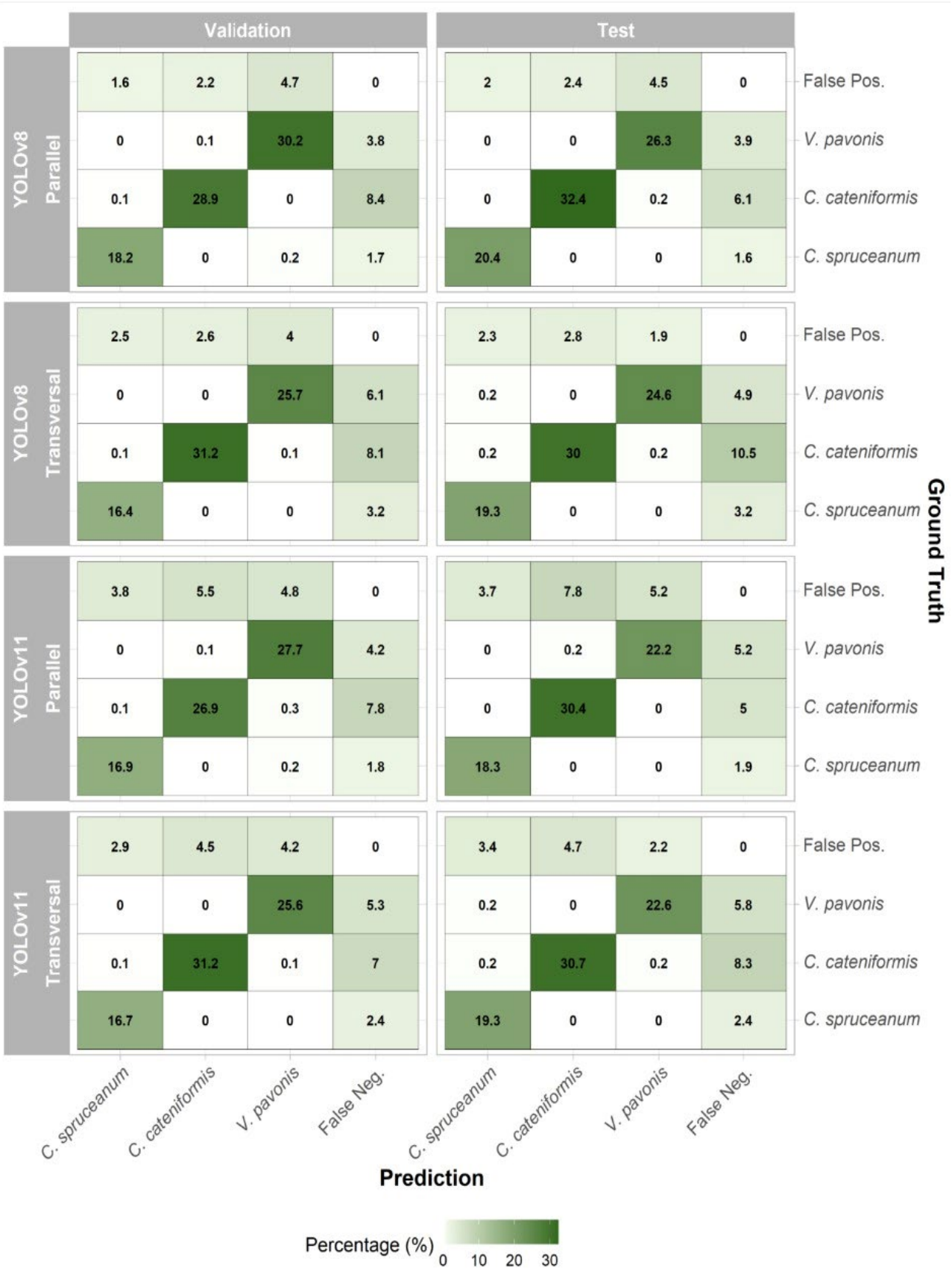

Figure 7. Confusion matrices (%) of YOLOv8 and YOLOv11 at 60 m drone flight height under parallel and transversal orientations, in validation (**left**) and test sets (**right**).

https://doi.org/10.3390/f17010087

3.4. Characterization of the Crown Morphology of Forest Species

The morphometric analysis revealed clearly differentiated structural patterns among the three evaluated species (Table 4). Regarding vertical structure, *C. spruceanum* consisted mainly of codominant individuals (55.1%), whereas *C. cateniformis* was dominated by trees in the dominant stratum (53.3%). In contrast, *V. pavonis* exhibited a predominance of suppressed individuals (49.4%).

Bifurcation position also showed marked contrasts: both *C. spruceanum* (46.9%) and *C. cateniformis* (78.3%) displayed a high frequency of bifurcation in the middle third of the crown, although this pattern was more pronounced in the latter. *V. pavonis*, on the other hand, was characterized by an almost complete absence of major bifurcations (96.3%).

Crown symmetry further distinguished the species. *C. spruceanum* and *V. pavonis* showed a strong tendency toward symmetric crowns (69.4% and 84%, respectively), whereas *C. cateniformis* had a slightly higher proportion of asymmetric crowns (54.3%), consistent with its laterally expansive growth form.

Branching angle also exhibited distinct patterns: *C. spruceanum* had almost exclusively acute-angled branches (98%), while *C. cateniformis* and *V. pavonis* were dominated by intermediate-angled branches (98.9% and 95.1%, respectively).

Finally, branch thickness showed a general tendency toward medium-sized branches across all species, although with different intensities: medium branches were predominant in *C. spruceanum* (63.3%), highly prevalent in *C. cateniformis* (81.5%), and also dominant in *V. pavonis* (65.4%). This latter species also exhibited the highest proportion of thin branches (34.6%), consistent with its reduced dominance within the canopy.

Table 4. Distribution of frequencies and percentages of tree crown morphological traits in an agroforestry system of the Peruvian Amazon.

Variable	Categories	*C. spruceanum*		*C. cateniformis*		*V. pavonis*	
		Frequency	Percentage	Frequency	Percentage	Frequency	Percentage
Vertical structure	Suppressed	3	6.12	0	0	40	49.4
	Intermediate	9	18.4	4	4.35	33	40.7
	Codominant	27	55.1	39	42.4	8	9.88
	Dominant	10	20.4	49	53.3	0	0
Bifurcation position	Bifurcation in lower third	0	0	0	0	0	0
	Bifurcation in middle third	23	46.9	72	78.3	1	1.23
	Bifurcation in upper third	14	28.6	19	20.7	2	2.47
	No bifurcation	12	24.5	1	1.09	78	96.3
Crown symmetry	Asymmetric crown	15	30.6	50	54.3	13	16
	Symmetric crown	34	69.4	42	45.7	68	84
Branching angle	Right-angled branches	0	0	0	0	3	3.7
	Acute-angled branches	48	98	1	1.09	1	1.23
	Intermediate-angled branches	1	2.04	91	98.9	77	95.1
Branch thickness	Thick branches	3	6.12	5	5.43	0	0
	Medium branches	31	63.3	75	81.5	53	65.4
	Thin branches	15	30.6	12	13	28	34.6

Multiple correspondence analysis (MCA) explained 36.2% of the variability in the data in the first two components (Component = 21.3%, Component = 14.9%; Figure 8). The qualitative traits of the crown produced a clear separation of the three species into partially distinct groups. *C. spruceanum* (Blue) was located predominantly in the upper part of the plot, associated with codominant individuals exhibiting acute branching angles, and bifurcation in the upper third, indicating a narrow, tall crown positioned in the upper canopy layer. *C. cateniformis* (Red) was concentrated in the lower-left zone of the plot,

associated with dominant trees characterized by asymmetric crowns, bifurcation in the middle third, and medium branch thickness, features typical of broad and laterally expansive crowns. *V. pavonis* clustered in the lower-right area of the biplot, linked to intermediate or suppressed individuals with symmetric crowns, absence of major bifurcation, and normally angled branches, representing a regular, balanced crown with lower vertical dominance.

Figure 8. Multiple Correspondence Analysis (MCA) Biplot of Crown Architecture: Species clustering based on vertical structure, crown symmetry, branching angle, bifurcation level, and branch thickness. Colored points represent individual trees, with each color corresponding to one of the three species (*C. spruceanum*, *C. cateniformis* and *V. pavonis*). Black triangular markers denote the categorical levels of the morphological variables included in the analysis. The ellipses illustrate the multivariate clustering patterns associated with each species.

4. Discussion

4.1. Effect of UAV Flight Parameters on Crown Segmentation Accuracy

A key finding of our study was that an intermediate flight height (~60 m) provided the highest crown segmentation accuracy. At this altitude, image resolution was sufficient to capture fine canopy-structural details, whereas flying lower (e.g., 40 m) did not yield further improvements. This pattern aligns with previous studies showing that segmentation accuracy increases as ground sampling distance (GSD) decreases, up to a point where higher resolutions no longer offer substantial benefits. For example, [11] reported that tree-crown detection accuracy peaks with high-resolution UAV imagery (a few centimeters per pixel) and declines once the GSD exceeds ~0.1 m. Similarly, [18] found that

detection performance was optimal when each crown occupied roughly 800–12,800 pixels, while overly coarse resolutions (<25 pixels) resulted in substantial crown omissions. Likewise, [61] documented that resampling UAV orthomosaics from 2 cm to 70 cm GSD progressively increased the discrepancies between segmented crown areas and ground-truth values. These results are consistent with the expectation that higher flight heights lose the fine canopy detail needed for accurate crown-boundary delineation. They also indicate diminishing returns at very low altitudes, a pattern similar to that reported by [62], who observed that flying at ~20 m tended to overestimate crown size, whereas an intermediate height of around 60 m was optimal for young oil palm stands.

In our study, we acquired exclusively nadir imagery and varied only the flight-line orientation (parallel vs. transversal). Under these controlled conditions, orientation had a secondary effect on crown delineation: the highest performance was obtained at 60 m, and within that height, parallel trajectories yielded slightly better results, although differences between orientations were generally modest. These variations can be attributed to the interaction between flight-path geometry and the structure of the agroforestry system. Parallel flights, which follow the row direction, tend to generate cleaner and more aligned crown footprints, as well as more homogeneous shadow patterns. This reduces the apparent overlap between neighboring crowns and facilitates boundary detection. In contrast, transversal flights accentuate cross-row overlap and produce more irregular shadow patterns, which likely explains the slight reduction in segmentation accuracy observed for this orientation. This behavior is consistent with [19], who demonstrated that aligning flight lines with the crop-row direction reduces motion blur and shadow occlusion, thereby improving canopy reconstruction. Similar importance of flight-path geometry has been highlighted in other UAV applications, such as construction-site inspection, where optimized flight-line planning enhances the quality of 3D reconstructions and reduces occlusions during aerial surveys [63].

Although our analyses focused exclusively on nadir imagery, complementary evidence suggests that the viewing angle also influences crown delineation. Several studies have shown that oblique imagery can be advantageous in complex or overlapping canopies, as it captures three-dimensional crown profiles that nadir views may overlook [64]. While oblique acquisition was not employed in this study, these findings point to a promising direction for future research in agroforestry systems with greater structural complexity, where integrating nadir and oblique perspectives could mitigate boundary ambiguity and reduce problems of under- and over-segmentation.

4.2. YOLOv8 vs. YOLOv11: Comparative Segmentation Performance

Several studies have demonstrated the potential of YOLO models for tree crown delineation using UAV imagery. For example, applying YOLOv5 to LiDAR data acquired by UAV achieved an F1-score of 0.74, outperforming traditional forest parameter–based methods [65]. Earlier versions, such as an enhanced YOLOv4 applied to canopy height models derived from LiDAR, reported recall and precision values of 83.6% and 81.4%, respectively [66], demonstrating their effectiveness for individual tree detection in forest environments. In this study, F1-score values were similar to or higher than those previously reported (Table 3), confirming the strong capability of YOLO models to accurately segment tree crowns in tropical agroforestry systems.

The comparison between YOLOv8 and YOLOv11 reveals a trade-off between maximum accuracy and consistency across conditions. YOLOv8 achieved the highest accuracy under optimal conditions (particularly at 60 m flight height and with parallel trajectories, where crown scale was ideal), with F1-scores near 0.88. However, its performance fluctuated notably with changes in height and orientation: at lower altitudes (40–50 m), where crowns appear larger and more overlapped, YOLOv8 showed substantial decreases in

accuracy. In contrast, YOLOv11 did not reach the maximum peak achieved by YOLOv8 but exhibited far more stable performance, maintaining F1-scores above 0.80 across most scenarios. This suggests that YOLOv11's architectural enhancements provide greater robustness to variations in image scale and viewpoint.

A fundamental difference between the two models lies in the design of the detection head. YOLOv8 uses an anchor-free approach, predicting object centers on a grid without predefined anchor boxes [67]. While this scheme can improve speed and localization for moderately sized objects, our results show that it struggles with small or densely overlapping crowns. This limitation has been documented in the literature; for example, Sun et al. [68] proposed YOLOv8E, a refined version designed to improve segmentation of small and medium-sized crowns in dense canopy structures. Conversely, YOLOv11 incorporates several architectural innovations, such as the C3k2 module, an improved SPPF neck, and a combined channel–spatial attention block (C2PSA), that enhance multiscale feature extraction and attention to relevant spatial details [69]. These improvements explain its greater stability and precision in detecting small or partially occluded crowns, as reflected in our experiments.

In summary, YOLOv11 addresses several of the limitations observed in YOLOv8. While YOLOv8 can achieve exceptional accuracy under ideal conditions, its sensitivity to scale and angle variations can lead to missed detections when crowns approach the limits of the model's resolution. Therefore, although YOLOv11 performed slightly below YOLOv8 in the ideal case (60 m, parallel flight), it consistently outperformed YOLOv8 in more challenging scenarios, which is particularly relevant for operational agroforestry monitoring, where drone flight conditions are not always constant.

Previous studies also support the suitability of YOLO detectors for this task. For instance, YOLOv3 was used to detect and measure pine crowns, achieving a high correspondence with ground-truth measurements ($R^2 \approx 0.94$) [70]. Similarly, YOLOv5-based models have outperformed traditional forestry algorithms relying on handcrafted features [65]. Recent literature also highlights efforts to improve YOLOv8 and YOLOv11 for crown detection. For example, an optimized YOLOv8 variant (YOLOv8E) achieved a mean Average Precision of 32.2% (AP50–95) on a complex urban forest dataset after modifying the model to address weaknesses in detecting small and overlapping crowns [68]. Likewise, an enhanced YOLOv11 variant (YOLOv11-OAM), which incorporated additional modules, achieved a notable 11.4% improvement in mAP@0.5, reaching 93.1% in a multi-species orchard dataset [69]. These findings confirm that, although both models are powerful, their performance can be significantly improved through domain-specific adaptations.

Deep learning models are known to exhibit sensitivity to random weight initialization, which can introduce variability in performance, particularly when training on relatively small datasets [71]. In this study, this potential source of variation was mitigated by initializing all models from COCO-pretrained weights and by applying consistent training protocols across all configurations. Moreover, the very low generalization gaps observed between validation and test sets (≤0.02 for YOLOv11 and ≤0.058 for YOLOv8) indicate stable model behavior across independent evaluation datasets, supporting the robustness of the reported results and suggesting that the main conclusions are not driven by random seed effects.

Although multiple independent training runs with different random seeds were not conducted, the consistency of the observed performance patterns across flight heights, flight orientations, and model architectures further supports the reliability of the comparative trends identified in this study. In particular, the identification of an optimal flight height and the contrasting behavior between YOLOv8 (higher peak accuracy but greater

variability) and YOLOv11 (slightly lower peak accuracy but higher stability) remained coherent across all evaluated configurations.

Crown segmentation methods based on canopy height models (CHMs) or 3D point clouds derived from LiDAR or photogrammetry, combined with techniques such as local maxima detection, watershed segmentation, or object-based image analysis, have been widely used [12,15,16,60,61,72]. However, these approaches typically require LiDAR data or high-quality photogrammetric reconstructions, as well as intensive parameter tuning. Moreover, our species-level differences confirm that crown morphology remains a limiting factor [12,60,72–74], indicating that YOLO-based approaches should be viewed as complementary tools rather than replacements for traditional methods in structurally complex agroforestry landscapes.

The visual analysis of the video obtained at a flight altitude of 60 m under parallel orientation revealed notable differences in segmentation behavior between the YOLOv8 and YOLOv11 models (Supplementary Video S1). The YOLOv8 model produced a smaller number of detections but with more defined contours that closely matched the actual crown boundaries, reflecting higher geometric precision and a lower incidence of over-segmentation. In contrast, YOLOv11 exhibited a greater number of detections and higher sensitivity to variations in texture and illumination, capturing partially shaded or densely overlapping crowns, although with a tendency toward boundary fusion and false detections in areas of high structural heterogeneity. These differences suggest that YOLOv8 emphasizes spatial specificity and morphological fidelity of individual crowns, whereas YOLOv11 prioritizes overall canopy coverage, providing broader detection at the expense of lower accuracy in individual tree delineation. Nevertheless, despite these differences, some crowns remained undetected by either model, highlighting the need for continued research to evaluate the generalization capacity and field efficiency of the developed models, as well as to explore methodological alternatives that could enhance accuracy in crown assessment and delineation.

4.3. Species-Specific Cup Morphology and Its Effect on Segmentation

In agroforestry systems, trees are often planted in more regular arrangements than in natural forests; however, the coexistence of multiple forest species with annual or perennial crops generates varying levels of competition for light, water, and nutrients. These interactions directly influence crown development, resulting in species-specific differences in crown area that must be captured through robust segmentation, as they are central to understanding both ecological dynamics and management outcomes.

Species-specific segmentation results align closely with previous research emphasizing that tree crown morphology, particularly crown shape, size, and isolation, is a primary determinant of detection accuracy, often exerting greater influence than sensor type or algorithm selection. Similar findings were reported by Gan et al. [11], who demonstrated that segmentation accuracy is strongly governed by crown shape. In their study of a temperate mixed forest, *Acer shirasawanum*, characterized by broad and horizontally spreading crowns, achieved the highest Mask R-CNN F1-scores, whereas *Acer nipponicum*, with a more compact and columnar crown, was detected with much lower accuracy. Despite sharing similar leaf morphology and taxonomic proximity, the two maple species differed markedly in segmentation success due to structural variation in crown architecture. Consistently, TLS-based analyses have shown that 3-D crown morphology can deviate substantially from simple allometric expectations as a function of neighborhood competition and species composition, further underscoring that fine-scale differences in crown architecture have disproportionate impacts on tree-level metrics and inference [75]

Consistent evidence is provided by Hastings et al. [72], who found that crown architecture significantly influences LiDAR-based mapping accuracy: automated methods

tended to perform well in conifer-dominated stands but were less reliable in closed-canopy broadleaf forests, where crown irregularity and overlap are more prevalent. Similar patterns were reported in a multi-ecosystem evaluation of a multi-layer LiDAR crown delineation algorithm, which detected overstory and understory trees more accurately in a structurally simpler conifer site than in a dense deciduous broadleaf forest, underscoring the sensitivity of individual-tree mapping to canopy complexity [73]. Conifers, with conical and symmetrical crowns, produce distinct canopy peaks and clear edges that facilitate delineation, whereas broadleaf species often exhibit flattened or fragmented crowns, leading to frequent over- and under-segmentation errors. Even in intensively managed orchards, irregular trained crowns require tailored UAV-based workflows to reliably extract crown width and projection area, highlighting again the challenges posed by non-standard crown shapes [74]. Similarly, reports on Prosopis species showed that trees with regular canopies exhibited smaller errors between conventional and LiDAR measurements [76].

In an agroforestry setting, *C. cateniformis* likely exhibited a degree of local crown shyness; as a taller emergent species, it avoids direct canopy contact with shorter neighboring trees, leaving a visible halo or outline in imagery. *C. spruceanum*, by contrast, appeared to lack such separation, its crowns commonly touched or overlapped adjacent trees. This interpretation aligns with findings by Sivanandam et al. [77], who emphasized that many tree detection methods rely on assumptions of uniformly spaced, non-overlapping crowns, and therefore perform poorly in heterogeneous, mixed-species forests. Similarly, LiDAR-based segmentation studies in multi-layered stands have shown that vertically overlapping crowns markedly reduce individual-tree detection rates because most algorithms implicitly assume a single, well-separated canopy surface [78].

At 60 m (parallel flight), Table 5 summarizes the crown morphology derived from the MCA for each species together with their segmentation metrics. Although the table does not directly demonstrate how vertical position or morphology determine performance, it does reveal consistent patterns that suggest associations between crown structure and model behavior. *C. cateniformis*, placed by the MCA in the left–lower quadrant (asymmetric crowns, mid-crown bifurcation, medium branches, many dominant individuals), exhibited broad, partly emergent canopies and delivered high AP@50 (YOLOv8 94/96; YOLOv11 94/97) with the lowest confusion for both models. *V. pavonis*, positioned in the right–lower quadrant (symmetric crowns, limited bifurcation, normal/right-angle branching), had regular, moderately dense crowns and intermediate AP@50 (YOLOv8 92/88; YOLOv11 91/89) with low–moderate cross-talk, slightly cleaner in YOLOv11. *C. spruceanum*, mapped to the upper half of the MCA (acute-angled branches; upper-third bifurcation; co-dominant), formed narrow, higher-tier crowns and achieved the highest AP@50 at this setting (YOLOv8 96/97; YOLOv11 97/98) yet showed more off-diagonal assignments than *C. cateniformis*, mainly boundary leakage into/out of *V. pavonis* when crowns are closely spaced.

Accumulating evidence shows that each forest or plantation type has its own structural configuration (in terms of composition, stratification and spatial pattern), which makes it necessary to conduct pilot studies to calibrate methods and validate assumptions at the local scale before upscaling their use. For example, Weinstein et al. [79] reported that when models were trained in one forest type and applied to another, performance generally decreased, with better results when forest structures were more similar. Similarly, Sun et al. [66] applied and validated a heightmap–deep learning approach in three plot types (nursery, forest landscape and mixed habitat), demonstrating that structural differences between plots affected crown detection and that on-site calibration and testing improved accuracy prior to scaling. In the same vein, Pucino et al. [80] showed that crown segmentation accuracy varies significantly among vegetation classes and that closed-

canopy forests pose different challenges than thinned areas, reinforcing the need to locally adjust methods and parameters through pilot studies.

Although this work focuses on a Peruvian Amazon agroforestry system, the UAV–YOLO framework that we develop is not specific to this region or to these three species. The selected species are representative of common functional roles and contrasting crown architectures in tropical agroforestry (dominant emergent crowns, narrow co-dominant crowns and intermediate symmetric crowns), so the methodological insights and recommended flight configurations are expected to be transferable to other tropical agroforestry systems, provided that models are retrained on locally representative imagery.

Table 5. Species-specific crown morphology (MCA), structural descriptors, AP@50, and model-separated confusion at 60 m (parallel flight lines).

Species	MCA-Derived Crown Traits (Per Dim1/Dim2)	Structural Description (from MCA Position)	YOLOv8 AP@50 (Val/Test, %)	YOLOv11 AP@50 (Val/Test, %)	Confusion @60 m—Parallel (YOLOv8)	Confusion @60 m—Parallel (YOLOv11)
C. spruceanum	Medium branches; acute branching angles; upper-third bifurcation; often co-dominant (upper half)	Narrow, higher-tier crown; smaller horizontal projection; greater canopy contact; edges can be irregular	96/97	97/98	Higher confusion than *C. cateniformis*: off-diagonal assignments to *V. pavonis*/*C. cateniformis* when crowns are closely spaced; typical error is boundary leakage/merging.	Higher confusion than *C. cateniformis* but generally less than YOLOv8: cross-class assignments persist at cluster edges; calibration is more stable.
C. cateniformis	Asymmetric crowns; mid-crown bifurcation (second third); medium branch thickness; many dominant (left–lower quadrant)	Broad, laterally expansive, partly emergent canopy; well-defined boundaries; crowns stand clear of neighbors	94/96	94/97	Lowest confusion: strong main diagonal; rare swaps (occasional into *V. pavonis*); robust to local crowding.	Lowest confusion: very clean diagonal; mislabels are rare/sporadic; slightly cleaner than YOLOv8.
V. pavonis	Symmetric crowns; no/limited major bifurcation; normal/right-angle branching; mostly intermediate/suppressed (right lower)	Balanced, regular crown outline; moderately dense mid–upper canopy; smooth boundaries	92/88	91/89	Moderate crosstalk: small bidirectional swaps with *C. cateniformis*; few errors into *C. spruceanum*; stable at parallel.	Low–moderate crosstalk: similar pattern but slightly reduced off-diagonal mass vs. YOLOv8.

5. Conclusions

This study shows that UAV flight height is the primary factor controlling individual tree crown (ITC) segmentation accuracy in a structurally heterogeneous agroforestry system of the Peruvian Amazon. An intermediate altitude of 60 m provided the best balance between crown detail and canopy coverage, yielding the highest F1-scores for both YOLOv8 and YOLOv11, whereas lower (40–50 m) and higher (70 m) altitudes produced more variable and slightly lower accuracies, in line with previous evidence on the joint

effects of ground sampling distance and crown size on ITC delineation. Flight orientation had a secondary influence: parallel flight lines generally outperformed transversal ones at the optimal height, but height clearly dominated the overall performance patterns.

The comparison between YOLOv8 and YOLOv11 revealed a trade-off between peak accuracy and robustness to changing acquisition conditions. YOLOv8 achieved the highest single-run test F1-score (≈0.886 at 60 m, parallel), but its performance and confidence-threshold calibration were more sensitive to flight height and orientation. YOLOv11 reached slightly lower peak F1-values but maintained an F1 > 0.80 and very small generalization gaps across most configurations, suggesting that YOLOv8 is preferable when flights can be tightly controlled around the optimal configuration, whereas YOLOv11 is better suited for operational monitoring where flight conditions are more heterogeneous.

Species-level analyses confirmed that crown morphology and vertical position strongly modulate segmentation difficulty. *Cedrelinga cateniformis*, with broad and partly emergent crowns, was segmented and classified with the highest accuracy, while *Calycophyllum spruceanum* and *Virola pavonis*, with narrower or more symmetric crowns and greater canopy contact, showed higher confusion, consistent with previous reports on the role of crown architecture and isolation in ITC delineation. Although our empirical results are anchored in a Peruvian Amazon case study, the proposed workflow, combining UAV-based RGB imagery, YOLO instance segmentation and crown morphological assessment, is generic and can be transferred to other tropical agroforestry systems and mixed-species forests, provided that models are retrained on locally representative data. Moreover, this pilot study provides a methodological foundation for future research explicitly aimed at evaluating the generalization of this approach across other agroforestry systems with broader structural variability and species composition. Future studies could explicitly incorporate repeated training with different random seed values and report average performance metrics together with measures of variability, in order to more accurately quantify the impact of stochastic initialization effects on model performance. They could also incorporate oblique or multi-angle imagery and evaluate the use of low-cost or multispectral LiDAR sensors to improve canopy segmentation and structural characterization in diverse agroforestry systems. Likewise, the broader application of these tools could support silvicultural management, including the planning of thinnings, pruning, and the phenotyping of seed trees.

Supplementary Materials: The following supporting information can be downloaded at: https://www.mdpi.com/article/10.3390/f17010087/s1, Figure S1: UAV-Based Workflow for Individual Tree Crown Segmentation in Agroforestry Systems; Figure S2: Training Dynamics of YOLOv8 and YOLOv11 at 60 m Flight Altitude under Parallel and Transversal Orientations; Figure S3: Variation of F1, Precision, and Recall with Confidence Threshold for YOLOv8 and YOLOv11 in Validation and Test Sets at 60 m Flight Altitude; Supplementary Video S1: Comparative Analysis of YOLOv8 and YOLOv11 Segmentation Efficiency in UAV Imagery Acquired from 60 m Parallel Flights (DOI: 10.17632/8swxxfrtd9.1).

Author Contributions: Conceptualization, J.R.B.-V., G.G.C. and P.Á.-Á.; methodology, J.R.B.-V., G.G.C., P.Á.-Á. and Z.H.I.; validation, J.R.B.-V., G.G.C., P.Á.-Á. and Z.H.I.; formal analysis, J.R.B.-V., G.G.C., P.Á.-Á. and Z.H.I.; investigation, J.R.B.-V., A.F.-S., S.F.P.F., E.J.S.-H., G.P.C.-R., R.P., J.R.H.D., G.A.T.C., G.V.-T. and G.G.C.; resources, A.F.-S., S.F.P.F., E.J.S.-H., G.P.C.-R., R.P., J.R.H.D., G.A.T.C., G.V.-T., G.G.C. and P.Á.-Á.; data curation, J.R.B.-V. and G.G.C.; writing—original draft preparation, J.R.B.-V. and G.G.C.; writing—review and editing, A.F.-S., S.F.P.F., E.J.S.-H., G.P.C.-R., R.P., J.R.H.D.; G.A.T.C., G.V.-T., G.G.C., P.Á.-Á. and Z.H.I.; visualization, A.F.-S., S.F.P.F., E.J.S.-H., G.P.C.-R., R.P., J.R.H.D., G.A.T.C., G.V.-T., G.G.C., P.Á.-Á. and Z.H.I.; supervision, P.Á.-Á. and Z.H.I.; project administration, J.R.B.-V., A.F.-S., S.F.P.F. and E.J.S.-H.; funding acquisition, A.F.-S.,

S.F.P.F., E.J.S.-H., G.P.C.-R., R.P., J.R.H.D., G.A.T.C. and G.V.-T. All authors have read and agreed to the published version of the manuscript.

Funding: This research was financed by the National Forestry Program of the National Institute for Agrarian Innovation and the "Programa Presupuestal 121—Mejora de la articulación de los pequeños productores a los mercados".

Data Availability Statement: The data presented in this study are available on request from the corresponding author (jrbasellyv@gmail.com).

Acknowledgments: The authors thank the technical team of the National Forestry Program of the San Roque Experimental Station for the support provided (Max Machoa Java, José Luis Teagua Paima, Roldán Campos, Hitoshi Pezo Macedo, Gebel Saisia Reategui Arevalo, Milagros Crystell Dossantos Macedo, Milca Vásquez Amasifuen and Kassandra Guerra Sánchez).

Conflicts of Interest: The authors declare that they have no conflicts of interest.

References

1. Echereme Chidi, B.; Mbaekwe Ebenezer, I.; Ekwealor Kenneth, U. Tree Crown Architecture: Approach to Tree Form, Structure and Performance: A Review. *Int. J. Sci. Res. Public* **2015**, *5*, 1–7.
2. Ritter, T.; Nothdurft, A. Automatic Assessment of Crown Projection Area on Single Trees and Stand-Level, Based on Three-Dimensional Point Clouds Derived from Terrestrial Laser-Scanning. *Forests* **2018**, *9*, 237. https://doi.org/10.3390/f9050237.
3. Scott-Brown, A.S.; Rial-Lovera, K.; Giannitsopoulos, M.L.; Rickson, J.R.; Staton, T.; Walters, K.F.A.; Burgess, P.J. Farmland Trees and Integrated Pest Management: A Review of Current Knowledge and Developing Strategies for Sustainable Systems. *Ecol. Solut. Evid.* **2025**, *6*, e70087. https://doi.org/10.1002/2688-8319.70087.
4. Zhang, D.; Du, G.; Sun, Z.; Bai, W.; Wang, Q.; Feng, L.; Zheng, J.; Zhang, Z.; Liu, Y.; Yang, S.; et al. Agroforestry Enables High Efficiency of Light Capture, Photosynthesis and Dry Matter Production in a Semi-Arid Climate. *Eur. J. Agron.* **2018**, *94*, 1–11. https://doi.org/10.1016/j.eja.2018.01.001.
5. Fleck, S.; Mölder, I.; Jacob, M.; Gebauer, T.; Jungkunst, H.F.; Leuschner, C. Comparison of Conventional Eight-Point Crown Projections with LIDAR-Based Virtual Crown Projections in a Temperate Old-Growth Forest. *Ann. Sci.* **2011**, *68*, 1173–1185. https://doi.org/10.1007/s13595-011-0067-1.
6. Owen, H.J.F.; Lines, E.R. Common Field Measures and Geometric Assumptions of Tree Shape Produce Consistently Biased Estimates of Tree and Canopy Structure in Mixed Mediterranean Forests. *Ecol. Indic.* **2024**, *165*, 112219. https://doi.org/10.1016/j.ecolind.2024.112219.
7. Getachew, M.T.; Zeleke, D.S. Aerodynamic Modeling and Performance Analysis of Model Predictive Controller for Fixed Wing Vertical Takeoff and Landing Unmanned Aerial Vehicle. *Eng. Res. Express* **2024**, *6*, 025548. https://doi.org/10.1088/2631-8695/ad4c61.
8. Andrade, H.J.; Segura, M.A. Dinámica de la sombra de *Cordia alliodora* en sistemas agroforestales con café en Tolima, Colombia. *Agron. Costarric.* **2016**, *40*, 77–86. https://doi.org/10.15517/rac.v40i2.27387.
9. Zhang, N.; Wang, Y.; Zhang, X. Extraction of Tree Crowns Damaged by *Dendrolimus tabulaeformis* Tsai et Liu via Spectral-Spatial Classification Using UAV-Based Hyperspectral Images. *Plant Methods* **2020**, *16*, 135. https://doi.org/10.1186/s13007-020-00678-2.
10. Bellow, J. Comparing Common Methods for Assessing Understory Light Availability in Shaded-Perennial Agroforestry Systems. *Agric. Meteorol.* **2003**, *114*, 197–211. https://doi.org/10.1016/S0168-1923(02)00173-9.
11. Gan, Y.; Wang, Q.; Iio, A. Tree Crown Detection and Delineation in a Temperate Deciduous Forest from UAV RGB Imagery Using Deep Learning Approaches: Effects of Spatial Resolution and Species Characteristics. *Remote Sens.* **2023**, *15*, 778. https://doi.org/10.3390/rs15030778.
12. Jiménez-Jiménez, S.I.; Ojeda-Bustamante, W.; Marcial-Pablo, M.; Enciso, J. Digital Terrain Models Generated with Low-Cost UAV Photogrammetry: Methodology and Accuracy. *ISPRS Int. J. Geoinf.* **2021**, *10*, 285. https://doi.org/10.3390/ijgi10050285.
13. Grybas, H.; Congalton, R.G. Evaluating the Impacts of Flying Height and Forward Overlap on Tree Height Estimates Using Unmanned Aerial Systems. *Forests* **2022**, *13*, 1462. https://doi.org/10.3390/f13091462.
14. Safonova, A.; Hamad, Y.; Dmitriev, E.; Georgiev, G.; Trenkin, V.; Georgieva, M.; Dimitrov, S.; Iliev, M. Individual Tree Crown Delineation for the Species Classification and Assessment of Vital Status of Forest Stands from UAV Images. *Drones* **2021**, *5*, 77. https://doi.org/10.3390/drones5030077.

15. Hosingholizade, A.; Erfanifard, Y.; Alavipanah, S.K.; Millan, V.E.G.; Mielcarek, M.; Pirasteh, S.; Stereńczak, K. Assessment of Pine Tree Crown Delineation Algorithms on UAV Data: From K-Means Clustering to CNN Segmentation. *Forests* **2025**, *16*, 228. https://doi.org/10.3390/f16020228.
16. Tinoco-Jaramillo, L.; Vargas-Tierras, Y.; Habibi, N.; Caicedo, C.; Chanaluisa, A.; Paredes-Arcos, F.; Viera, W.; Almeida, M.; Vásquez-Castillo, W. Agroforestry Systems of Cocoa (*Theobroma cacao* L.) in the Ecuadorian Amazon. *Forests* **2024**, *15*, 195. https://doi.org/10.3390/f15010195.
17. Díaz, M.; Alegre, J.; Gómez, C.; García, C.; Arévalo-Hernández, C. Effect of Light on Yield, Nutritive Value of *Brachiaria decumbens*, and Soil Properties in Silvopastoral Systems, Peruvian Amazon. *Grasses* **2025**, *4*, 18. https://doi.org/10.3390/grasses4020018.
18. Hao, Z.; Lin, L.; Post, C.J.; Mikhailova, E.A.; Yu, K.; Fang, H.; Liu, J. The Co-Effect of Image Resolution and Crown Size on Deep Learning for Individual Tree Detection and Delineation. *Int. J. Digit. Earth* **2023**, *16*, 3753–3771. https://doi.org/10.1080/17538947.2023.2257636.
19. Tu, Y.-H.; Phinn, S.; Johansen, K.; Robson, A.; Wu, D. Optimising Drone Flight Planning for Measuring Horticultural Tree Crop Structure. *ISPRS J. Photogramm. Remote Sens.* **2020**, *160*, 83–96. https://doi.org/10.1016/j.isprsjprs.2019.12.006.
20. Redmon, J.; Divvala, S.; Girshick, R.; Farhadi, A. You Only Look Once: Unified, Real-Time Object Detection. In Proceedings of the IEEE Conference on Computer Vision and Pattern Recognition, Las Vegas, NV, USA, 27–30 June 2016; pp. 779–788.
21. Terven, J.; Córdova-Esparza, D.-M.; Romero-González, J.-A. A Comprehensive Review of YOLO Architectures in Computer Vision: From YOLOv1 to YOLOv8 and YOLO-NAS. *Mach. Learn. Knowl. Extr.* **2023**, *5*, 1680–1716. https://doi.org/10.3390/make5040083.
22. Shen, L.; Lang, B.; Song, Z. DS-YOLOv8-Based Object Detection Method for Remote Sensing Images. *IEEE Access* **2023**, *11*, 125122–125137. https://doi.org/10.1109/ACCESS.2023.3330844.
23. Sharma, A.; Kumar, V.; Longchamps, L. Comparative Performance of YOLOv8, YOLOv9, YOLOv10, YOLOv11 and Faster R-CNN Models for Detection of Multiple Weed Species. *Smart Agric. Technol.* **2024**, *9*, 100648. https://doi.org/10.1016/j.atech.2024.100648.
24. Ayturan, K.; Sarıkamış, B.; Akşahin, M.F.; Kutbay, U. SPHERE: Benchmarking YOLO vs. CNN on a Novel Dataset for High-Accuracy Solar Panel Defect Detection in Renewable Energy Systems. *Appl. Sci.* **2025**, *15*, 4880. https://doi.org/10.3390/app15094880.
25. Wang, X.; Zhao, Q.; Jiang, P.; Zheng, Y.; Yuan, L.; Yuan, P. LDS-YOLO: A Lightweight Small Object Detection Method for Dead Trees from Shelter Forest. *Comput. Electron. Agric.* **2022**, *198*, 107035. https://doi.org/10.1016/j.compag.2022.107035.
26. Qiu, Q.; Lau, D. Assessment of Trees' Structural Defects via Hybrid Deep Learning Methods Used in Unmanned Aerial Vehicle (UAV) Observations. *Forests* **2024**, *15*, 1374. https://doi.org/10.3390/f15081374.
27. Wang, H.; Zhang, Y.; Zhu, C. YOLO-LFD: A Lightweight and Fast Model for Forest Fire Detection. *Comput. Mater. Contin.* **2025**, *82*, 3399–3417. https://doi.org/10.32604/cmc.2024.058932.
28. Jarahizadeh, S.; Salehi, B. Advancing Tree Detection in Forest Environments: A Deep Learning Object Detector Approach with UAV LiDAR Data. *Urban For. Urban Green.* **2025**, *105*, 128695. https://doi.org/10.1016/j.ufug.2025.128695.
29. Zhorif, N.N.; Anandyto, R.K.; Rusyadi, A.U.; Irwansyah, E. Implementation of Slicing Aided Hyper Inference (SAHI) in YOLOv8 to Counting Oil Palm Trees Using High-Resolution Aerial Imagery Data. *Int. J. Adv. Comput. Sci. Appl.* **2024**, *15*, 869–874. https://doi.org/10.14569/IJACSA.2024.0150786.
30. Araújo Júnior, C.A.; Oliveira, L.S.D.; Eça, G.A. Counting of Shoots of *Eucalyptus* Sp. Clones with Convolutional Neural Network. *Pesqui. Agropecu. Bras.* **2023**, *58*, e03363. https://doi.org/10.1590/s1678-3921.pab2023.v58.03363.
31. Casas, G.G.; Ismail, Z.H.; Limeira, M.M.C.; da Silva, A.A.L.; Leite, H.G. Automatic Detection and Counting of Stacked Eucalypt Timber Using the YOLOv8 Model. *Forests* **2023**, *14*, 2369. https://doi.org/10.3390/f14122369.
32. Casas, G.G.; Ismail, Z.H.; Limeira, M.M.C.; Soares, C.P.B.; Gleriani, J.M.; Binoti, D.H.B.; Araújo Júnior, C.A.; Shapiai, M.I.; Rodrigues, L.I.; Araújo, T.M.; et al. Quantifying Solid Volume of Stacked Eucalypt Timber Using Detection-Segmentation and Diameter Distribution Models. *Smart Agric. Technol.* **2024**, *9*, 100653. https://doi.org/10.1016/j.atech.2024.100653.
33. Sánchez-Vega, J.A.; Silva-López, J.O.; Salas Lopez, R.; Medina-Medina, A.J.; Tuesta-Trauco, K.M.; Rivera-Fernandez, A.S.; Silva-Melendez, T.B.; Oliva-Cruz, M.; Barboza, E.; da Silva Junior, C.A.; et al. Automatic Detection of Ceroxylon Palms by Deep Learning in a Protected Area in Amazonas (NW Peru). *Forests* **2025**, *16*, 1061. https://doi.org/10.3390/f16071061.
34. Velasquez-Camacho, L.; Etxegarai, M.; de-Miguel, S. Implementing Deep Learning Algorithms for Urban Tree Detection and Geolocation with High-Resolution Aerial, Satellite, and Ground-Level Images. *Comput Env. Urban Syst* **2023**, *105*, 102025. https://doi.org/10.1016/j.compenvurbsys.2023.102025.

35. Meza López, A.; Cornelius, J.P. *La Agroforestería en Perú, Con Énfasis en la Amazonía: Una Bibliografía Anotada*; World Agroforestry Centre: Nairobi, Kenya, 2006.
36. Kristanto, Y.; Tarigan, S.; June, T.; Sulistyantara, B.; Wijayanti, P. Designing Agroforestry Cacao to Implement Multifunctional Landscapes by Synergizing Ecosystem Service and Economic Value1. *Trees For. People* **2025**, *21*, 100974. https://doi.org/10.1016/j.tfp.2025.100974.
37. Tito, R.; Salinas, N.; Cosio, E.G.; Boza Espinoza, T.E.; Muñiz, J.G.; Aragón, S.; Nina, A.; Roman-Cuesta, R.M. Secondary Forests in Peru: Differential Provision of Ecosystem Services Compared to Other Post-Deforestation Forest Transitions. *Ecol. Soc.* **2022**, *27*, art12. https://doi.org/10.5751/ES-13446-270312.
38. Rikolto. Amazonas: Agroforestry Systems Secure Soils and Ecosystems for Peruvian Cocoa. Available online: https://www.rikolto.org/stories/amazonas-agroforestry-systems-secure-soils-and-ecosystems-for-peruvian-co-coa#:~:text=In%202020%2C%20APROCAM%20launched%20its,the%20soil%2C%20and%20the%20ecosystem (accessed on 28 August 2025).
39. Nash, J.; Grewer, U.; Bockel, L.; Galford, G.; Pirolli, G.; White, J. *Peru Cacao Alliance: Carbon Sequestration as a Co-Benefit of Cacao Expansion*; CCAFS Info Note; CCAFS: Wageningen, The Netherlands, 2016.
40. Parodi, A.; Villamonte-Cuneo, G.; Loboguerrero, A.M.; Martínez-Barón, D.; Vázquez-Rowe, I. Embedding Circularity into the Transition towards Sustainable Agroforestry Systems in Peru. *Sci. Total Environ.* **2022**, *838*, 156376. https://doi.org/10.1016/j.scitotenv.2022.156376.
41. Vallejos-Torres, G.; Gaona-Jimenez, N.; Pichis-García, R.; Ordoñez, L.; García-Gonzales, P.; Quinteros, A.; Lozano, A.; Saavedra-Ramírez, J.; Tuesta-Hidalgo, J.C.; Reategui, K.; et al. Carbon Reserves in Coffee Agroforestry in the Peruvian Amazon. *Front. Plant. Sci.* **2024**, *15*, 1410418. https://doi.org/10.3389/fpls.2024.1410418.
42. Chávez, J.M.R.; Sebbenn, A. Genetic Control of Quantitative and Qualitative Traits of *Calycophyllum spruceanum* in the Peruvian Amazon. *Crop Breed. Appl. Biotechnol.* **2024**, *24*, e47262419. https://doi.org/10.1590/1984-70332024v24n1a09.
43. Sotelo Montes, C.; Vidaurre, H.; Weber, J. Variation in Stem-Growth and Branch-Wood Traits among Provenances of *Calycophyllum spruceanum* Benth. from the Peruvian Amazon. *New For.* **2003**, *26*, 1–16.
44. Baselly-Villanueva, J.R.; Fernández-Sandoval, A.; Salazar-Hinostroza, E.J.; Cárdenas-Rengifo, G.P.; Puerta, R.; Trigoso, T.S.C.; Rufasto-Peralta, Y.L.; Vallejos-Torres, G.; Casas, G.G.; Araújo Junior, C.A.; et al. MultiProduct Optimization of *Cedrelinga cateniformis* (Ducke) Ducke in Different Plantation Systems in the Peruvian Amazon. *Forests* **2025**, *16*, 164. https://doi.org/10.3390/f16010164.
45. Barneby, R.C.; Grimes, J.W. *Silk Tree, Guanacaste, Monkey's Earring: A Generic System for the Synandrous Mimosaceae of the Americas. Part I. Abarema, Albizia, and Allies*, 1st ed.; The New York Botanical Garden: Bronx, NY, USA, 1996; Volume 74.
46. Murga-Orrillo, H.; Pashanasi Amasifuén, B.; Arévalo López, L.A.; Inuma, M.C.; Abanto-Rodríguez, C. *Cedrelinga catenaeformis* (Tornillo) in Natural and Agroforestry Systems: Dendrometry, Soil and Macrofauna. *Trees For. People* **2024**, *16*, 100577. https://doi.org/10.1016/j.tfp.2024.100577.
47. González-Rodríguez, M.; Ruiz-Fernández, C.; Francisco, V.; Ait Eldjoudi, D.; Farrag AbdElHafez, Y.R.; Cordero-Barreal, A.; Pino, J.; Lago, F.; Campos-Toimil, M.; Rocha Carvalho, G.; et al. Pharmacological Extracts and Molecules from Virola Species: Traditional Uses, Phytochemistry, and Biological Activity. *Molecules* **2021**, *26*, 792. https://doi.org/10.3390/molecules26040792.
48. SENAMHI. Mapa Climático del Perú. Available online: https://www.senamhi.gob.pe/main.php?dp=loreto&p=mapa-climatico-del-peru (accessed on 28 October 2025).
49. Cardenas-Rengifo, G.P.; Baselly-Villanueva, J.R.; Chumbimune-Vivanco, S.Y.; Macedo-Ramírez, A.T.; Salazar, E.; Minaya, B.; Quintana, S.; Cabudivo, A.; Palma, S.S.A.; Álvarez-Álvarez, P.; et al. Using Acoustic Tomography to Model Wood Deterioration in *Cedrelinga cateniformis* Ducke in the Peruvian Amazon. *Forests* **2024**, *15*, 778. https://doi.org/10.3390/f15050778.
50. Cruz, W.; Saldaña, C.; Ramos, H.; Baselly, R.; Cancán Loli, J.; Cuellar, E. Genetic Structure of Natural Populations of *Cedrelinga cateniformis* "tornillo" from the Oriental Region of Peru. *Sci. Agropecu.* **2020**, *11*, 521–528. https://doi.org/10.17268/sci.agropecu.2020.04.07.
51. DJI. Support for DJI Mini 3 Pro. Available online: https://www.dji.com/global/support/product/photo (accessed on 28 October 2025).
52. Dronelink. Dronelink | Mission Planner. Available online: https://www.dronelink.com/mission-planner (accessed on 28 October 2025).
53. Gallagher, J. Launch: Train Larger Models on Roboflow. Available online: https://blog.roboflow.com/train-larger-models-on-roboflow/ (accessed on 27 August 2025).

54. Corley, I.; Robinson, C.; Dodhia, R.; Ferres, J.M.L.; Najafirad, P. Revisiting Pre-Trained Remote Sensing Model Benchmarks: Resizing and Normalization Matters. In Proceedings of the IEEE/CVF Conference on Computer Vision and Pattern Recognition (CVPR) Workshops, Seattle WA, USA, 17–21 June 2024; pp. 3162–3172.
55. Ultralytics Inc. COCO Dataset—Ultralytics YOLO Docs. Available online: https://docs.ultralytics.com/datasets/detect/coco (accessed on 27 August 2025).
56. R Core Team. *R: A Language and Environment for Statistical Computing*; R Foundation for Statistical Computing: Vienna, Austria, 2020.
57. Wickham, H. *Ggplot2*; Springer International Publishing: Cham, Switzerland, 2016; ISBN 978-3-319-24275-0.
58. Galera Peral, R.M.; Martín Albertos, S.; Alía Miranda, R.; Gordo Alonso, J.; Aguado Ortega, A.M.; Notivol Paino, E. *Manual de Selección de Masas Productoras de Semillas. Evaluación de Caracteres*; Instituto Nacional de Investigación y Tecnología Agraria y Alimentaria: Madrid, Spain, 1997.
59. Kong, F.; Bi, H.; McLean, M.; Li, F. Comparative Performances of New and Existing Indices of Crown Asymmetry: An Evaluation Using Tall Trees of *Eucalyptus pilularis* (Smith). *J. Res.* **2021**, *32*, 43–65. https://doi.org/10.1007/s11676-020-01180-0.
60. Kassambara, A.; Mundt, F. Factoextra: Extract and Visualize the Results of Multivariate Data Analyses. R Package Version 1.0.7.999. 2020. Available from: https://github.com/kassambara/factoextra (accessed on 9 November 2025).
61. Hosingholizade, A.; Erfanifard, Y.; Alavipanah, S.K.; Latifi, H.; Jouybari-Moghaddam, Y. Tree crown delineation on UAV imagery using combination of machine learning algorithms with majority voting. *ISPRS Ann. Photogramm. Remote Sens. Spat. Inf. Sci.* **2023**, *X-4/W1-2022*, 287–293. https://doi.org/10.5194/isprs-annals-X-4-W1-2022-287-2023.
62. Avtar, R.; Suab, S.A.; Syukur, M.S.; Korom, A.; Umarhadi, D.A.; Yunus, A.P. Assessing the Influence of UAV Altitude on Extracted Biophysical Parameters of Young Oil Palm. *Remote Sens.* **2020**, *12*, 3030. https://doi.org/10.3390/rs12183030.
63. Liu, X.; Yi, W.; Chen, P.; Tan, Y. Flight Path Planning of UAV-Driven Refinement Inspection for Construction Sites Based on 3D Reconstruction. *Autom. Constr.* **2025**, *177*, 106360. https://doi.org/10.1016/j.autcon.2025.106360.
64. Lei, L.; Yin, T.; Chai, G.; Li, Y.; Wang, Y.; Jia, X.; Zhang, X. A Novel Algorithm of Individual Tree Crowns Segmentation Considering Three-Dimensional Canopy Attributes Using UAV Oblique Photos. *Int. J. Appl. Earth Obs. Geoinf.* **2022**, *112*, 102893. https://doi.org/10.1016/j.jag.2022.102893.
65. Straker, A.; Puliti, S.; Breidenbach, J.; Kleinn, C.; Pearse, G.; Astrup, R.; Magdon, P. Instance Segmentation of Individual Tree Crowns with YOLOv5: A Comparison of Approaches Using the ForInstance Benchmark LiDAR Dataset. *ISPRS Open J. Photogramm. Remote Sens.* **2023**, *9*, 100045. https://doi.org/10.1016/j.ophoto.2023.100045.
66. Sun, C.; Huang, C.; Zhang, H.; Chen, B.; An, F.; Wang, L.; Yun, T. Individual Tree Crown Segmentation and Crown Width Extraction from a Heightmap Derived from Aerial Laser Scanning Data Using a Deep Learning Framework. *Front. Plant Sci.* **2022**, *13*, 914974. https://doi.org/10.3389/fpls.2022.914974.
67. Terven, J.; Cordova-Esparza, D. A Comprehensive Review of YOLO: From YOLOv1 to YOLOv8 and Beyond. *arXiv* **2023**, arXiv:2304.00501. https://doi.org/10.48550/arXiv.2304.00501.
68. Sun, Z.; Xue, B.; Zhang, M.; Schindler, J. YOLOv8E: An Efficient YOLOv8 Method for Instance Segmentation of Individual Tree Crowns in Wellington City, New Zealand. *J. R. Soc. N. Z.* **2025**, *55*, 1854–1879. https://doi.org/10.1080/03036758.2024.2424802.
69. Wang, Q.; Pu, Z.; Luo, L.; Wang, L.; Gao, J. A Study on Tree Species Recognition in UAV Remote Sensing Imagery Based on an Improved YOLOv11 Model. *Appl. Sci.* **2025**, *15*, 8779. https://doi.org/10.3390/app15168779.
70. Lou, X.; Huang, Y.; Fang, L.; Huang, S.; Gao, H.; Yang, L.; Weng, Y.; Hung, I.-K. uai Measuring Loblolly Pine Crowns with Drone Imagery through Deep Learning. *J. For. Res.* **2022**, *33*, 227–238. https://doi.org/10.1007/s11676-021-01328-6.
71. Barz, B.; Denzler, J. Deep Learning on Small Datasets without Pre-Training Using Cosine Loss. In Proceedings of the IEEE/CVF Winter Conference on Applications of Computer Vision (WACV), Snowmass Village, CO, USA, 1–5 March 2020; pp. 1371–1380.
72. Hastings, J.H.; Ollinger, S.V.; Ouimette, A.P.; Sanders-DeMott, R.; Palace, M.W.; Ducey, M.J.; Sullivan, F.B.; Basler, D.; Orwig, D.A. Tree Species Traits Determine the Success of LiDAR-Based Crown Mapping in a Mixed Temperate Forest. *Remote Sens.* **2020**, *12*, 309. https://doi.org/10.3390/rs12020309.
73. Duncanson, L.I.; Cook, B.D.; Hurtt, G.C.; Dubayah, R.O. An Efficient, Multi-Layered Crown Delineation Algorithm for Mapping Individual Tree Structure across Multiple Ecosystems. *Remote Sens. Env.* **2014**, *154*, 378–386. https://doi.org/10.1016/j.rse.2013.07.044.
74. Mu, Y.; Fujii, Y.; Takata, D.; Zheng, B.; Noshita, K.; Honda, K.; Ninomiya, S.; Guo, W. Characterization of Peach Tree Crown by Using High-Resolution Images from an Unmanned Aerial Vehicle. *Hortic. Res.* **2018**, *5*, 74. https://doi.org/10.1038/s41438-018-0097-z.

75. Owen, H.J.F.; Flynn, W.R.M.; Lines, E.R. Competitive Drivers of Interspecific Deviations of Crown Morphology from Theoretical Predictions Measured with Terrestrial Laser Scanning. *J. Ecol.* **2021**, *109*, 2612–2628. https://doi.org/10.1111/1365-2745.13670.
76. Chumbimune-Vivanco, S.Y.; León, H.; Llanos-Carrillo, C.; Millan-Ramírez, J.; Vilca-Gamarra, C.; Vera, E.; Agurto, A.; Baselly-Villanueva, J.R.; Cruz-Grimaldo, C. Integration of VANT-LiDAR with Multispectral Imagery for the Estimation of Carbon Stocks in Prosopis Sp. Forest Plantations. *Sci. Agropecu.* **2025**, *16*, 333–348. https://doi.org/10.17268/sci.agropecu.2025.025.
77. Sivanandam, P.; Lucieer, A. Tree Detection and Species Classification in a Mixed Species Forest Using Unoccupied Aircraft System (UAS) RGB and Multispectral Imagery. *Remote Sens.* **2022**, *14*, 4963. https://doi.org/10.3390/rs14194963.
78. Hamraz, H.; Contreras, M.A.; Zhang, J. Vertical Stratification of Forest Canopy for Segmentation of Understory Trees within Small-Footprint Airborne LiDAR Point Clouds. *ISPRS J. Photogramm. Remote Sens.* **2017**, *130*, 385–392. https://doi.org/10.1016/j.isprsjprs.2017.07.001.
79. Weinstein, B.G.; Marconi, S.; Bohlman, S.A.; Zare, A.; White, E.P. Cross-Site Learning in Deep Learning RGB Tree Crown Detection. *Ecol Inf.* **2020**, *56*, 101061. https://doi.org/10.1016/j.ecoinf.2020.101061.
80. Pucino, N.; McVicar, T.; Levick, S.; van Dijk, A. The Accuracy of Image-Based Individual Tree Crown Detection and Delineation across Vegetation Types. *Int. Arch. Photogramm. Remote Sens. Spat. Inf. Sci.* **2025**, *XLVIII-G-2025*, 1223–1227. https://doi.org/10.5194/isprs-archives-XLVIII-G-2025-1223-2025.